ELECTRON SPIN RESONANCE AND ELECTRON-SPIN-ECHO STUDY OF ORIENTED MULTILAYERS OF L_α-DIPALMITOYLPHOSPHATIDYLCHOLINE WATER SYSTEMS

LEELA KAR, EVA NEY-IGNER, AND JACK H. FREED
Department of Chemistry, Baker Laboratory, Cornell University, Ithaca, New York 14853

ABSTRACT A detailed electron spin resonance (ESR) study of spin-labeled–oriented multilayers of L_α-dipalmitoylphosphatidylcholine (DPPC) water systems for low water content (2–10% by weight) is reported with the purpose of characterizing the dynamical and structural properties of model membrane systems. Emphasis is placed on the value of combining such experiments with detailed simulations based on current slow-motional theories. Information is obtained regarding ordering and anisotropic rotational diffusion rates via ESR lineshape analysis over the entire motional range, from the fast motional region through the moderately slow and slow to the rigid limit. This includes the low-temperature gel phase, the liquid crystalline $L_\alpha(1)$ phase and what appears to be a third high-temperature phase above the L_α phase. Cholestane (CSL) and spin-labeled DPPC (5-PC, 8-PC, and 16-PC) have been used to probe different depths of the bilayer. While CSL and 5-PC both reflect the high ordering of the bilayer close to the lipid-water interface, CSL appears to be located close enough to the water for the nitroxide to be involved in hydrogen bonding with water molecules. 16-PC reflects the relatively low ordering near the tail of the hydrocarbon chain in the bilayer. Quantitative estimates of ordering and motion are obtained for these cases. The results from CSL indicate that close to the lipid-water interface the DPPC molecule is oriented approximately perpendicular to the bilayer in these low water-content systems. However, all three labeled lipid probes indicate that the hydrocarbon chain of DPPC may be bent away from the bilayer normal by as much as 30° and this evidence is stronger at low temperatures. When cholesterol is added to the DPPC-water system at a concentration $\geq$2.5 mol %, the ordering is greatly increased although the rotational diffusion rate remains almost unaffected in the gel phase. Electron spin echoes (ESE) are observed for the first time from oriented lipid-water multilayers. Results obtained from cw ESR lineshape analysis are correlated with data from ESE experiments, which give a more direct measurement of relaxation times. These results indicate that for detection of very slow motions (close to the rigid limit) ESE experiments are more sensitive to dynamics than continuous wave ESR for which inhomogeneous broadening becomes a major problem.

INTRODUCTION

Electron spin resonance (ESR) studies of spin probes dissolved in liquid crystals have been used to characterize both the dynamic behavior of the solute (probe molecule) and the structure and properties of the surrounding solvent (the liquid crystalline medium) (1–12). Thermotropic liquid crystalline phases studied in this lab have led to the understanding of several properties of solute and solvent molecules (1–11); these include anisotropic diffusion, anisotropic viscosity, deviations from Brownian reorientation, effects due to fluctuating torques, and slowly relaxing local structure. Lyotropic systems, like the lipid-water system, have been the subject of a large number of investigations with the purpose of obtaining information regarding dynamics and structure of these model membrane systems in their different phases (13). Techniques used in such investigations include x-ray (14–16), electron (17), and neutron (18) diffraction, electron microscopy (19–20), Raman spectroscopy (21, 22), differential scanning calorimetry (23, 24), nuclear magnetic resonance (25, 26), and ESR (27–29). The vast quantity of work done in this area in the past two decades has generated a large amount of data, some contradictions, and numerous interesting observations that require explanation. Most of the investigations, including the ESR studies, have been performed on lipid-water dispersions. Information obtained from ESR studies of dispersions lacks the resolution obtainable from well-oriented samples where one has macroscopic as well as microscopic ordering. The effect of orientation becomes significant for lipid-water systems since they exhibit lyotropic smectic phases, so one has the additional experimen-

tal degree of freedom of tilting the external magnetic field relative to the director. We wished to apply our experience in ESR studies of thermotropic smectic phases, where we used a variety of spin probes and well-developed theories for analyzing ESR lineshapes, to lyotropic smectic phases of lipid-water systems. We report here ESR studies of spin probes in well-oriented multilayers of partially hydrated L_α-dipalmitoylphosphatidylcholine (DPPC).

Previous reports from this lab (30, 31) have described the initial success, both in alignment of oriented multilayers of partially hydrated DPPC and in the use of advanced computational techniques to analyze continuous wave (cw) ESR spectra of various spin probes in such oriented multilayers. Along with several interesting results, these studies point to the importance of verifying the degree of alignment of each multilayer sample by independent means in order to interpret correctly the ESR results. For example, ESR lineshapes similar to those obtained with a periodic distribution of directors (30) (described by a $(\sin\theta)^{-1}$ function, implying long-range cooperative chain distortions) could be obtained if it were assumed that the sample was partially misaligned (8) (Fig. 1). A similar interpretation based on misalignment has been reported for oriented films of hydrated phospholipids (32). We have attempted to resolve such ambiguities using polarizing microscopy to detect macroscopic defects present in samples used for ESR data collection.

This paper describes the preparation of largely defect free, low water content, oriented lipid-water multilayer samples suitable for ESR studies. We report on the changes in structure and dynamics at the molecular level brought about by varying the temperature, thickness, and water content, and by the incorporation of cholesterol in these oriented phospholipid multilayers. Successful alignment of thick samples (100 to 400 μm in thickness) enabled us to have sufficient signal to detect ESE for the first time from these oriented lipid systems. We discuss below the importance of ESE experiments in guiding and complementing cw ESR lineshape studies in such systems. Methods of sample preparation and other relevant experimental details are described in the Experimental section. Next data analysis and results are discussed, followed by a further discussion of results and a summary.

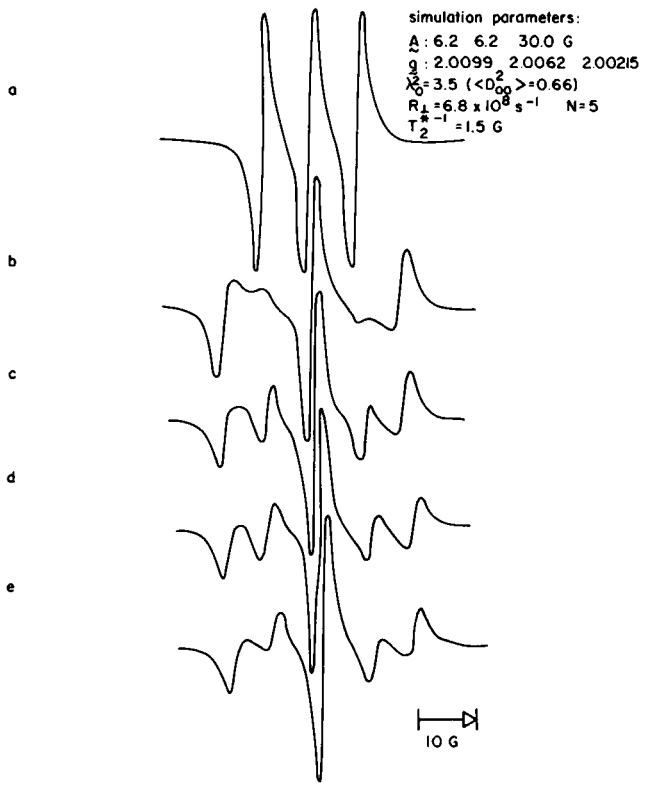

FIGURE 1 Illustration of ambiguity in interpretation of ESR spectra of nitroxides. *d* shows an experimental ESR spectrum obtained using CSL in DPPC containing 2 wt % water at 107°C (reference 30). Spectra *a*, *b*, *c*, and *e* have been simulated using the parameters shown in the figure and the following additional conditions: (*a*) assuming no macroscopic disorder to be present; (*b*) assuming microscopic order and macroscopic disorder to be present and describing the macroscopic disorder by a random distribution of directors; (*c*) assuming 76% macroscopic disorder to be superimposed on 24% well-oriented sample; (*e*) assuming a periodic distribution of directors to be present, described by a $(\sin\theta)^{-1}$ function, implying long-range cooperative chain distortion.

EXPERIMENTAL

Preparation of Oriented Multilayers

We use the techniques of Powers and Pershan (33–35) and Asher and Pershan (36) as guidelines. Their techniques primarily consist of a thermal annealing of defect structures formed in lipid-water multilayers sandwiched between two glass plates. Large aligned monodomain samples are produced (>125 μm thick × 1 cm^2 area). For the purpose of ESR study we not only required larger samples (containing sufficient numbers of spins for a reasonable signal-to-noise ratio), we also needed to make certain that the sample remained defect free over long periods of time during which ESR data are collected. Some modifications in the preparation technique were, therefore, necessary. In general, however, similarities between our observations during the annealing procedure and those of Powers et al. and Asher et al. show that the basic methodology remains the same. Anhydrous DPPC was obtained from Sigma Chemical Corp. (St. Louis, MO) and used without further purification. Its purity was checked from time to time with thin-layer chromatography (TLC).

A uniform mixture of the anhydrous lipid, spin label, and any additive (e.g., cholesterol) is obtained by slow evaporation under low vacuum ($\sim 10^{-2}$ torr) of a solution containing these components in the appropriate ratios. Since benzene is easily removed, it is usually used as the common solvent, a few drops of ethanol being added, if required. After evaporation, dry nitrogen gas is passed over the mixture to ensure removal of all traces of solvents. A microsyringe is used to add the appropriate amount of water (percent by weight) directly to the mixture, stirring thoroughly to aid uniform distribution of the water. This mixture is then sealed in an inert atmosphere (of dry nitrogen or argon) and left at room temperature for 48 to 72 h so that hydration of the phospholipids reaches equilibrium. Glass plates cut to size (0.7 cm × 3 cm) from No. 1 or No. 2 thickness of microscope cover glass, are cleaned thoroughly, and coated with the surfactant hexadecyl-trimethylammonium bromide (HTAB, Eastman Kodak Co., Rochester, NY), to aid homeotropic alignment of the phospholipid. A small amount of the hydrated phospholipid is then sandwiched between the surfactant-coated surfaces of the glass plates. The sandwich is placed between two standard microscope slides and uniform pressure is applied by means of pinchcock clamps, making sure that the slides remain parallel. Any excess material escaping under

pressure from the sides of the sandwich is removed with a razor blade. All four edges of the sandwich are then sealed with epoxy (extra fast setting epoxy from Hardman, Belleville, NJ). Thickness of the sandwich is varied simply by varying the amount of sample placed between the coated plates. Alternatively, Mylar strips of varying thickness could be used as spacers. However, the former method is more suitable both for sample alignment and for proper packing of the sample to reduce air pockets in the sandwich. To minimize water loss, the sample is prepared at room temperature and sealed as quickly as possible. Gravimetric measurements show that, between the addition of water and preparation of the sealed sandwich, the water concentration remains within 10% of its initial value. Once sealed, the sandwich sample may be stored in the refrigerator for a few days without any detrimental effects. At this stage, depending on the thickness, water content, and additives used, the sandwich sample may look powdery, opaque, or even transparent at room temperature. Examination under a polarized microscope, however, shows that even the transparent samples are not completely aligned. Application of shear stress at slightly elevated temperatures (instead of perpendicular pressure at room temperature) appears to improve the alignment to some extent. However, at temperatures below the gel-to-L_α transition temperature, pressure alone does not appear to align these thick samples. Defect structures that seem to appear spontaneously during the preparation of these hydrated multilayers have to be thermally annealed as described below.

The annealing procedure uses a FP52 automatic temperature control unit (Mettler Instrument Corp., Hightstown, NJ) in conjunction with a polarizing microscope (Nikon Inc., Instrument Div., Garden City, NY). The sandwich sample is heated within the microfurnace of the FP52 unit at the rate of 1° to 2°C/min. Transmittance of polarized light through the sample (with polarizers in the crossed position) is monitored using a photodiode and a x-t chart recorder. The sample temperature is increased until a relatively sharp decrease in transmittance indicates the formation of homeotropically aligned domains in the region of the sample within the field of view. The temperature is then either maintained constant or carefully raised by a few degrees until homeotropic alignment is achieved throughout, and the entire sample appears dark when scanned between crossed polars. The maximum temperature required for this to occur ranges from 100° to 140°C and appears to depend on sample composition and thickness. (For these samples the optically isotropic phase appears at $T \gtrsim 160$°C). The sample temperature is then lowered to room temperature at a rate slow enough to maintain the homeotropic alignment achieved at high temperature (2 to 1°C/min). The entire heating and cooling cycle usually takes 2 to 3 h. During this annealing process, while the sample temperature remains above the L_α-to-gel transition temperature, many of the smaller aligned domains merge to form larger ones. However, our samples remain multidomain in character, boundaries becoming visible as the temperature is lowered. Both defect formation (or failure to anneal away defect structures) and the presence of trapped air pockets lead to the formation of domains.

Our microscopic observations during the thermal annealing process are very similar to those reported by Asher and Pershan (36). Defect structures were not studied in any detail, but were noted mainly to compare our sample preparation technique with other reported techniques. Only those samples that contained <10% of macroscopically disordered regions (as confirmed later from ESR spectra and their subsequent analysis) were used for data collection. Fig. 2 shows some examples of variation of transmittance of polarized light with temperature. The curves corresponding to the first heating cycle are similar to those reported by Sakurai and Iwayanagi (17) for a hydrated powder specimen of DPPC, and these curves reflect changes in water content (Fig. 2 *a,b*). On reversing the temperature the transmittance curve is not reversed, but remains more or less flat. We had hoped that the transmittance would indicate the final water content of the aligned sample (on completion of the thermal annealing process) by marking the onset of in-plane optical anisotropy at the L_α-to-gel phase transition. However, the shape of the curve corresponding to the cooling cycle seems to depend

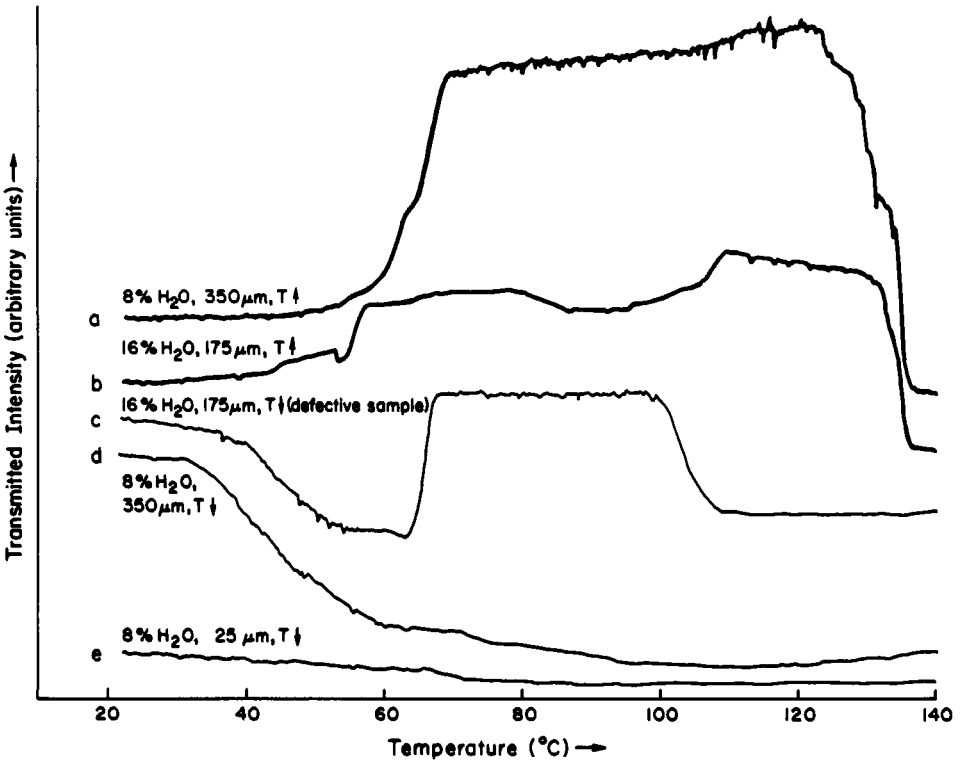

FIGURE 2 Illustration of variation of transmittance of polarized light with sample temperature for DPPC-water multilayers. *a* and *b* (thick lines) show the transmittance curves corresponding to increasing temperature during the thermal annealing process, while *c*, *d*, and *e* (thin lines) show the transmittance curves corresponding to decreasing temperature. See text for discussion.

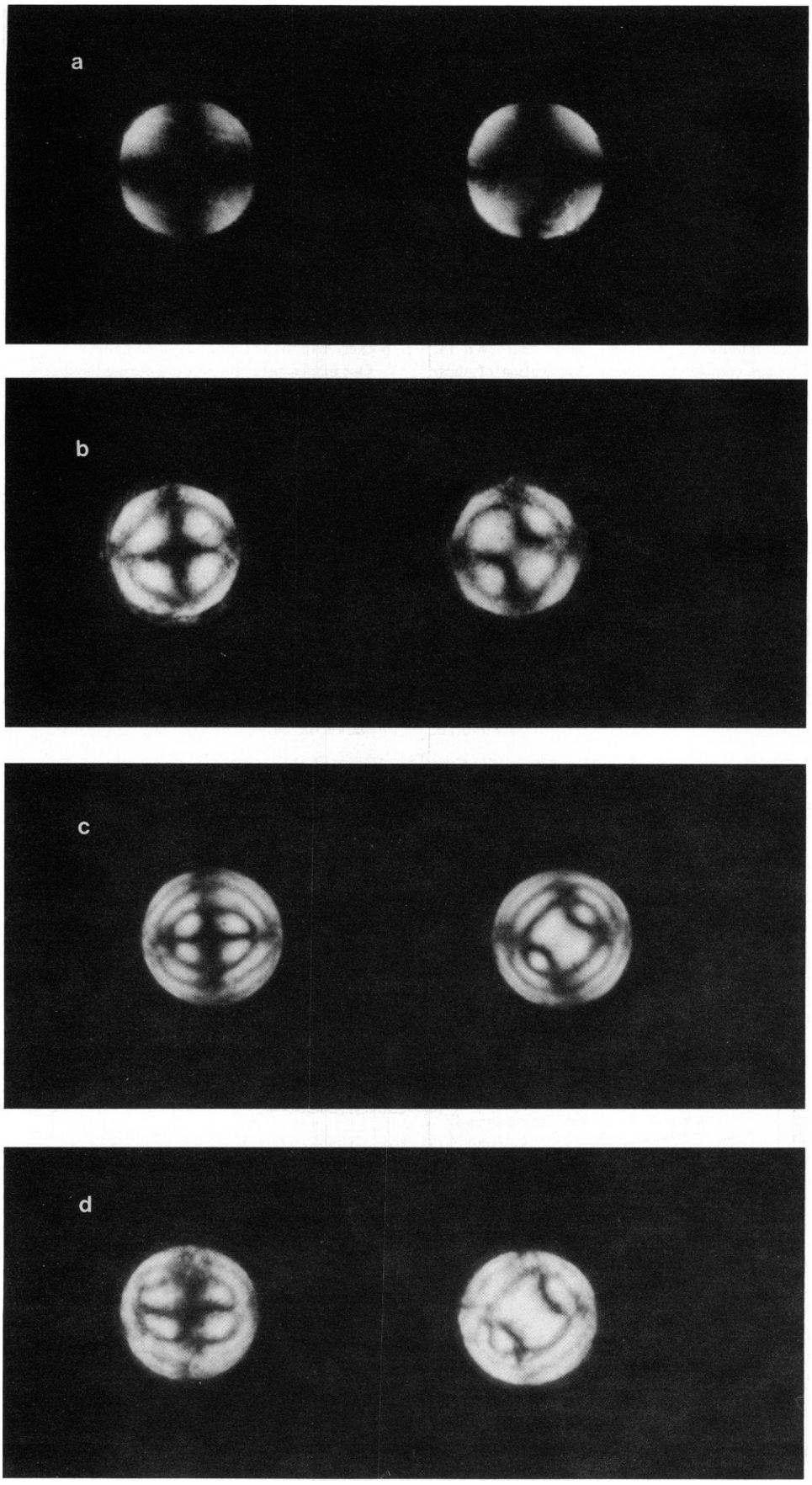
a
b
c
d

more upon sample thickness, amount of defects present, and number of domains (or boundary regions) present in the field of view. For practically defect free thin samples (~25 μm) the transmittance changed very little over the temperature range from 140 to 23°C (Fig. 2 *e*). For thick samples (200 to 400 μm), the gel transition is indicated by an increase in transmittance (Fig. 2 *d*) as reported by Sakurai and Iwayanagi for their layered crystals of L-DPPC dihydrate (17), except that for our plate samples the change is very gradual (over a temperature range of ~30°C, compared with ~10°C for the L-DPPC crystals). If defects are present (>10%) the transmittance curve corresponding to the cooling cycle (Fig. 2 *c*) contains features observed in the curves for the heating cycle, implying the presence of random molecular orientations. The differences in these curves may be qualitatively explained as follows. Once the molecules have been aligned at high temperatures, the transmittance curve during the cooling cycle essentially monitors changes in optical anisotropy in the bilayer plane brought about by molecular structural changes, for example, in the side-by-side packing of molecules. In the absence of such alignment, i.e., for a polycrystalline or powderlike sample, the transmittance mainly reflects structural changes in the direction of the largest refractive index, which is along the chain direction, perpendicular to the bilayer. Phase transition temperatures indicated by ESR spectra showed the water content of all our samples to be within 2 to 10% by weight. There is, therefore, considerable loss of water (through the epoxy seal or the epoxy-glass interface) during the thermal annealing process and the alignment technique had to be modified for high water content samples. Here we only report experiments performed with low water content samples, aligned at elevated temperatures as described above. The water content of the samples was estimated by proton nuclear magnetic resonance (NMR) of samples treated similarly but containing no spin label.[1]

Conoscopy performed at 23°C showed all samples to be biaxial at this temperature (Fig. 3), confirming the reduction of water content to <10% (35). Conoscopy was used only qualitatively, as a simple visual check on sample homogeneity and thickness and showed that samples aligned at high temperatures remained aligned on cooling. TLC performed following the annealing process showed no degradation of the lipid. Comparison of ESR spectra before and after annealing showed no detectable reduction of spin concentration for the experiments reported here.

Using the technique described above we were able to align lipid multilayers of low water content (~2 to ~10%). We have successfully aligned partially hydrated multilayers of DPPC, DMPC, a 1:1 mixture of DPPC and DMPC, and egg lecithin. We were also able to align samples containing various concentrations of cholesterol (~2.5 to 33 mol %). In general, thin samples (≤100 μm) were easier to align and contained fewer defects than thick samples (≥100 μm), which were required for ESE experiments. Addition of cholesterol also increased the difficulty in achieving alignment. A qualitative estimation of sample alignment could be obtained both by polarizing microscopy and by ESR. The primary type of defect obtained is one of macroscopic disorder. For a poorly aligned sample in the smectic phase, the ESR spectrum obtained with the mean director parallel to the external magnetic field shows a typical three line nitroxide spectrum (Fig. 4 *b*) with the two extra peaks at the high and low field ends (Fig. 4 *c*) corresponding to the macroscopic defect. Simulations using a random distribution of directors to represent the defect show that such macroscopic disorder of ≥10% is easily detectable in the ESR spectra (Fig. 4 *c*). The spectra from aligned samples remain reversible throughout the temperature range studied (−150 to 130°C). When studied under a polarizing microscope, however, some of the thick samples showed the appearance of defects (described as "polygonal array defects" by Asher and Pershan [36]) on heating to the $L_\alpha(1)$ phase. Their effects on the ESR spectra may be only small changes in linewidth and are therefore not detectable except upon careful lineshape analysis. The formation of these defect structures was suppressed when the sample was cooled carefully from an elevated temperature (120–130°C). All ESR data collection was therefore performed during the cooling cycle only. Aligned and properly sealed samples of low water-content lipid-water multilayers may be stored in the refrigerator for several months. (In fact, ESR spectra were found to be reproducible after 2 y.) These samples were always heated to the high-temperature phase ($T \geq 110$°C) before observations were made on them.

The amount of macroscopic defect formed in a sample after the first thermal annealing cycle often may be reduced by repeated heating and cooling between 120 and 25°C (Fig. 5). The second cycle usually reduces the amount of defect to ≤10%. Cycles following this have little effect on the alignment and some fraction of the originally formed defect always remains. However, most samples are virtually free of macroscopic defects (≤10%) after the first thermal annealing. Alignment by repeated heating/cooling cycles is generally avoided for fear of water loss during successive annealing cycles even though for low water-content samples (2 to 10%) this water loss is very small (36).

Conoscopy shows that multilayer thickness varies within the same sample, i.e., the thickness of the multilayer is not equal to the gap between the two glass plates throughout the sample (see Fig. 3). This is true for most thick samples (≥100 μm) where it is difficult to pack the starting material homogeneously and thereby avoid trapping air within the sample sandwich. However, as shown in the next section, varying multilayer thickness (within ~25 to 350 μm) has no significant effect on the ESR spectra.

Spin Labels

Cholestane (CSL) was prepared by Dr. Eva Ney-Igner, Cornell University, Ithaca, NY. The nitroxide-labeled DPPC (5-PC, 8-PC, and 16-PC) was obtained from Professor G. W. Feigenson of the Department of Biochemistry and Molecular Cell Biology at Cornell University, Ithaca, NY. The concentration of spin labels was increased in steps from 10^{-4} M and found to have no observable effect on linewidth of ESR spectra until

[1]The sandwich was broken after the annealing process and the DPPC-water mixture extracted using deuterated solvents (a 2:1 mixture of C_6D_6 and $CDCl_3$) to prepare a suitable NMR sample. NMR spectra were observed on a Varian CFT-20 pulsed spectrometer (Varian Associates, Inc., Palo Alto, CA). The signal corresponding to the water was compared with that of the —N—$(CH_3)_3$ group of the lipid, both before and after the annealing process.

FIGURE 3 Conoscopy observed at 23°C using oriented samples of low water content DPPC (i.e., after thermal annealing). The cross position is shown on the left while the figure obtained by a 45° rotation from this position (of the microscope stage holding the sample) is shown on the right. In *a*, *b*, and *c* the thickness of the sample (or the number of bilayers) under the crossed polars is varied. As the thickness is increased (from *a* to *c*) the number of rings observed in the conoscopic figure increases, and the hyperbolic figure corresponding to the 45° position (*right*) becomes more resolved. All three (*a*, *b*, *c*) of these figures may be observed using different parts of the same sample, showing that multilayer thickness (or number of bilayers present) may vary from domain to domain in these multidomain plate samples. *d* shows the blurred conoscopic figures obtained from an originally oriented sample that was left for a month at ~25°C. Although polarizing microscopy at 25°C does not show any observable defects, polygonal array structures are usually seen on reheating these samples to $T \geq 100$°C. Repeating the thermal annealing process (i.e., heating to 120 or 130°C and carefully cooling to 25°C) suppresses these defect structures and the sharp conoscopic figures shown in *c* are observed. Note that the cross on the left rotates to a hyperbola on the right in every case (*a*, *b*, *c*, *d*), showing the samples to be biaxial at 25°C. (It is difficult to observe this change for thin samples as in *a*.) The cross would remain unchanged upon rotation of the sample for an uniaxial system.

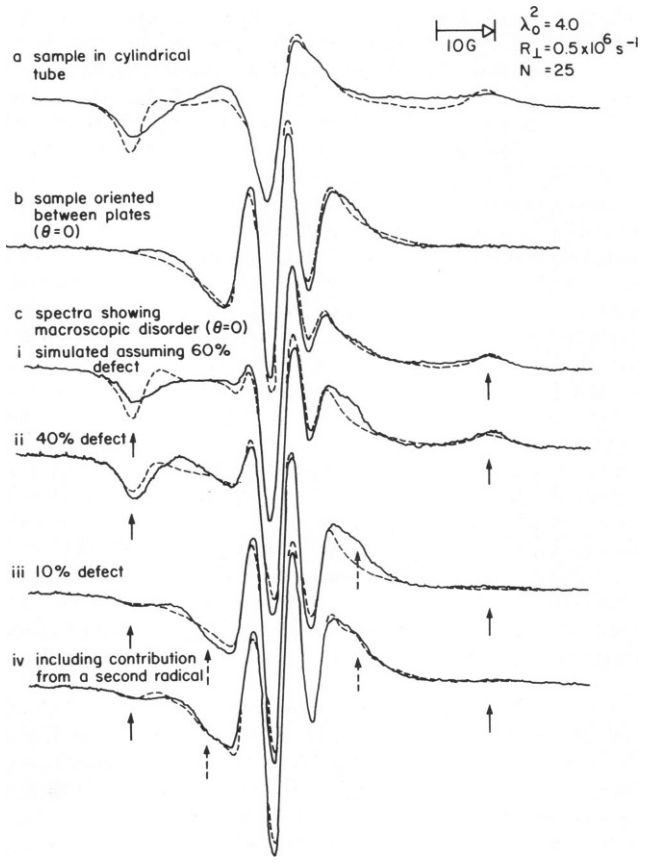

FIGURE 4 Experimental (solid line) and simulated (broken line) ESR spectra at 22°C for CSL in DPPC with ~4 wt % water. (*a*) Sample is in a cylindrical tube, i.e., macroscopically unoriented. Simulation assumes presence of microscopic order and a random distribution of directors. (*b*) Sample is oriented between plates and positioned with the plate normal parallel to the external magnetic field. Simulation assumes both microscopic and macroscopic order. (*c*) Spectra from plate samples containing various amounts of defects after thermal annealing. All spectra are for $\theta = 0°$ orientation. Simulations assume superposition of macroscopic disorder or defect (as in *a*) on a spectrum with both microscopic and macroscopic order (as in *b*). Position of extra peaks due to defects are marked with solid arrows. Agreement between simulated and experimental spectra improve on inclusion of contribution from a second radical species (peaks marked with broken arrows). See Fig. 13 and the Analysis and Results section entitled Studies Using CSL for discussion.

increased to 10^{-2} M. Most of the experiments were performed with samples containing 10^{-3} M or 5×10^{-3} M of spin label. Degassing of samples as described earlier (30, 31) was not found to be necessary for our purpose. Fig. 6 shows the molecular formulae of spin labels used in this work.

Instrumentation

CW ESR measurements were performed on a Varian E-12, X-band spectrometer (Varian Associates, Inc., Palo Alto, CA) using 100-kHz field modulation. The sample temperature was varied between 130°C and −150°C using a Varian E-257 variable temperature control unit (Varian Associates, Inc.). A copper-constantan thermocouple was used to measure the sample temperature to an accuracy of ±1° in absolute value.

The ESE set-up used has been described elsewhere (37). Phase memory time, T_M, was measured as a function of sample temperature and orientation in the external magnetic field. All T_M measurements were performed with the external magnetic field corresponding to the $M = 0$ line for the nitroxides. A 90°-τ-180° echo sequence was used, with a 90° pulse width of 80 ns. Although observable echoes were obtained using a single sample, several (up to 5) sample sandwiches packed side by side were sometimes used for a stronger signal.

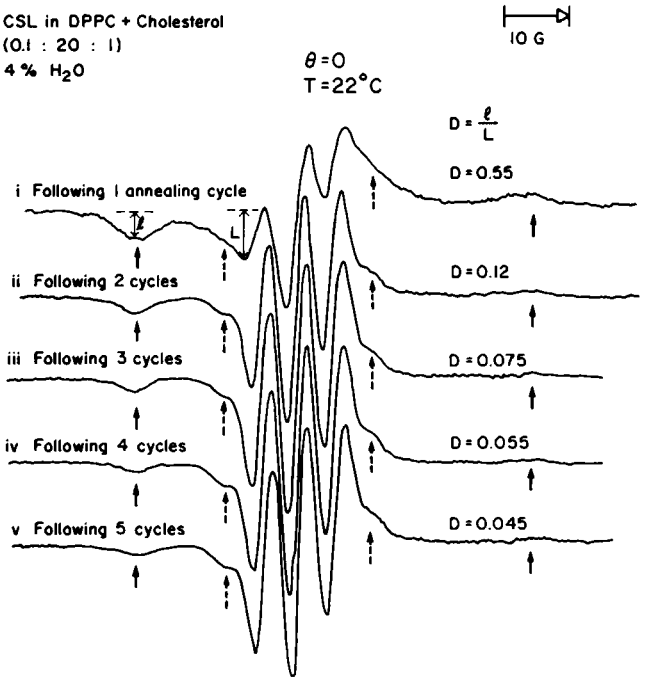

FIGURE 5 Experimental spectra illustrating the effect of several cycles of thermal annealing on an originally defective sample. See text for discussion.

ANALYSIS AND RESULTS

The results reported here mainly involve studies using CSL as the spin bearing probe molecule and these are described in the next section. Results from studies using spin-labeled DPPC (5-PC, 8-PC, 16-PC) are included in the next section only when necessary for lending support to the CSL studies. In the section entitled Studies Using the PC Probes a few specific results of the labeled-DPPC studies are discussed to emphasize the large range of information obtainable when different spin labels are used to probe the same system. The section entitled ESE Experiments contains results of the spin echo experiments. Notation used is as in references 30 and 31.

Studies Using CSL

ESR spectra obtained from well-aligned DPPC-water samples containing CSL are characteristic of spectra from highly ordered anisotropic media (9–11, 38–42). Although such spectra have been observed before using CSL in oriented lipid-water systems (38–42), a detailed lineshape analysis has not yet been reported. Also, sample alignment techniques used in previous investigations were different from our study and may have resulted in significant amounts of sample mosaicity (32). Recent refinements of the Polnaszek, Bruno, and Freed (PBF) theory and the

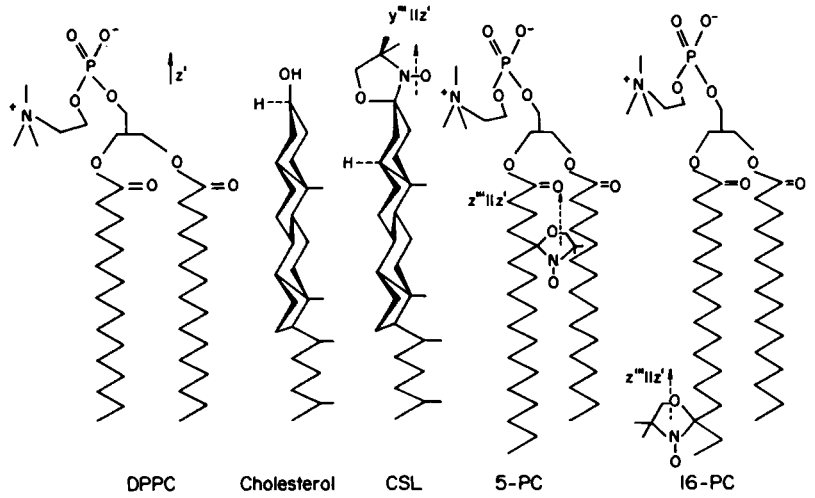

FIGURE 6 Molecular formulae and schematic structures for DPPC, cholesterol, CSL, 5-PC, and 16-PC. The axis, z', of the set of molecular ordering axes (x', y', z') has been related to the magnetic axes (x''', y''' z''') according to the geometry predicted by ESR spectral simulations.

efficient use of the Lanczos algorithm to reduce computation time (1–4) have enabled the present detailed analysis of the very complex ESR lineshapes obtained from these lipid-water systems, especially at low temperatures ($T < 50$°C).

The spectra show smectic A symmetry as illustrated in Fig. 7. This symmetry is observed with all four spin probes (CSL, 5-PC, 8-PC, 16-PC) within the temperature range -150°C $< T <$ 130°C. Change in water content (between ~2% to ~10% by weight) and addition of cholesterol both leave the smectic A symmetry unchanged. Implications of this with regard to hydrocarbon chain tilt are discussed later in this section.

Spectral features remain unaffected by changes in sample thickness (i.e., number of bilayers between the glass plates) between ~25 and ~400 μm (Fig. 8). By our alignment technique, therefore, we are able to maintain long-range cooperativity between bilayers up to several thousand bilayers. Also Fig. 8 shows that ESR spectral features remain reproducible from sample to sample when all conditions (except sample thickness) are unchanged, reflecting the reproducibility of the sample preparation procedure itself.

Magnetic Parameters. The magnetic parameters $A_{x'''}$, $A_{y'''}$, $A_{z'''}$ and $g_{x'''}$, $g_{y'''}$, $g_{z'''}$ were estimated with the help of rigid limit spectra at very low temperatures (5). Both tube and plate samples were cooled to -150°C. $A_{z'''}$ and $g_{z'''}$ were determined experimentally from rigid limit spectra observed using tube samples (5). However, the central part of the spectra was poorly resolved due to proton inhomogeneous broadening. Therefore, the x''' and

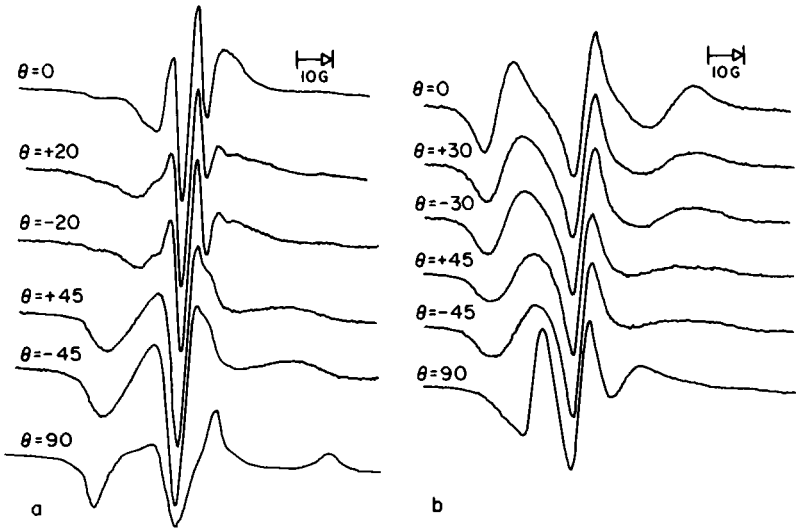

FIGURE 7 Experimental ESR spectra from low water content, oriented samples of DPPC containing (*a*) CSL, (*b*) 16-PC. θ denotes the angle between the static field and the normal to the glass plate. The spectra illustrate smetic A symmetry, i.e., spectra at θ and $\pi - \theta$ (or $-\theta$) are identical.

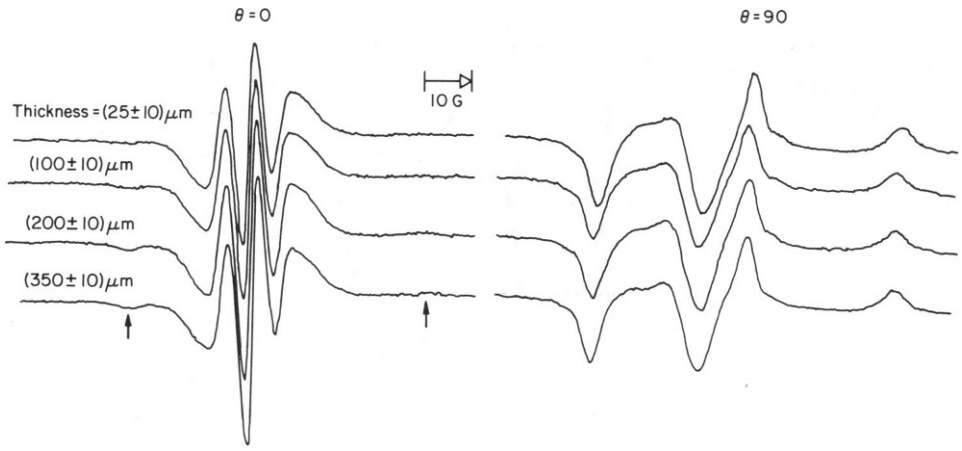

FIGURE 8 Experimental ESR spectra from oriented samples of ~4 wt % water content DPPC containing ~5×10^{-3} M CSL. Average bilayer thickness has been varied. Positions of extra peaks in the $\theta = 0$ spectrum due to macroscopic disorder present in the samples are marked with arrows.

y''' components of A and g tensors could not be determined unambiguously from experiment. On cooling the plate samples, macroscopic ordering was preserved and the rigid limit spectra in this case were orientation dependent. The $g_{z'''}$ value determined experimentally from tube samples was found to be very close to the published value for CSL in single crystals of cholestryl chloride (45, 46), $\{g_z$ (DPPC + 4% H_2O) = 2.0019 ± 0.00017, g_z(cholestryl chloride) = 2.0021$\}$. The best estimate of the $g_{y'''}$ value from the orientation-dependent rigid limit spectra observed using plate samples (2.0056 ± 2.0002) was also close to that for CSL in cholestryl chloride. Hence the principal values of the g tensor reported for CSL in cholestryl chloride was used for our calculations. The isotropic values A_{iso} (=14.5 ± 0.1 G) and g_{iso} (= 2.0060 ± 0.00017) were measured by heating a sample containing CSL to the isotropic phase (>160°C for 2% water content). Since the measured $A_{z'''}$ value of 33.6 ± 0.5 G was different from the reported 31.9 G for CSL in cholestryl chloride, values for $A_{x'''}$ and $A_{y'''}$ were estimated assuming axial symmetry and using the relationship $A_\perp = A_{x'''} = A_{y'''} = 1/2\,(3A_{iso} - A_{z'''}) \simeq$ 5.0 G. The best estimate for $A_\perp$ from the orientation-dependent rigid limit spectra was 4.8 G, close to the calculated value above. These estimated values for $A_{x'''}$, $A_{y'''}$, and $A_{z'''}$ were used as starting values for spectral simulations and modified as required for best fit. In simulating rigid limit spectra from tube samples the relevant variables are the A and g tensors. Simulation of rigid limit spectra from plate samples requires additional parameters to describe the ordering potential. However, since these spectra from macroscopically ordered samples are orientation dependent, there is also greater resolution of information. The combination of rigid limit spectra from both tube and plate sample therefore increases one's confidence with parameters estimated from these spectra. Fig. 9 shows the experimental and best fit simulated spectra for CSL in DPPC at −150°C for both tube and plate samples. A similar procedure was used to estimate magnetic parameters corresponding to the other three probes (5-PC, 8-PC, and 16-PC). Table I lists the magnetic parameters used for spectral simulations for the different spin labels.

Spectral Simulations. Fig. 10 shows examples of experimental and simulated spectra for CSL in DPPC in the temperature range 20°C < T < 130°C. It was assumed that the liquid crystalline medium is uniaxial and that the most important terms in the Wigner matrix expansion of the ordering potential U are those of second rank (6):

$$U(\Omega) = \lambda_0^2 D_{00}^2(\Omega) + (\lambda_2^2 + \lambda_{-2}^2)\,[D_{20}^2(\Omega) + D_{-20}^2(\Omega)],$$

where Ω is the set of Eulerian angles relating the molecular frame (principal axes of ordering and diffusion for the probe molecule) and the director frame. The order parameters $\langle D_{00}^2 \rangle$ and $\langle D_{20}^2 + D_{-20}^2 \rangle$ are defined by

$$\langle D_{00}^2 \rangle = \frac{\int \delta\Omega \exp\,[-U(\Omega)/kT]\, D_{00}^2(\Omega)}{\int \delta\Omega \exp\,[-U(\Omega)/kT]}$$

$$\langle D_{20}^2 + D_{-20}^2 \rangle = \frac{\int \delta\Omega \exp\,[-U(\Omega)/kT]\,(D_{20}^2 + D_{-20}^2)}{\int \delta\Omega \exp\,[-U(\Omega)/kT]}.$$

Reasonable agreement between theory and experiment was obtained in most cases with a single term axially symmetric potential of the form

$$P(\Omega) = \frac{\exp\,[-U(\Omega)/kT]}{\int \exp\,[-U(\Omega)/kT]\delta\Omega},$$

where $U(\Omega)$ is proportional to $\lambda_0^2 D_{00}^2(\Omega)$.

A model of Brownian diffusion, with an axially symmetric diffusion tensor diagonal in the molecular frame, with $R_\parallel$ and $R_\perp$ denoting, respectively, the principal values along, and perpendicular to, the main symmetry axis, gave fairly good fits. The asymmetry parameter N was defined

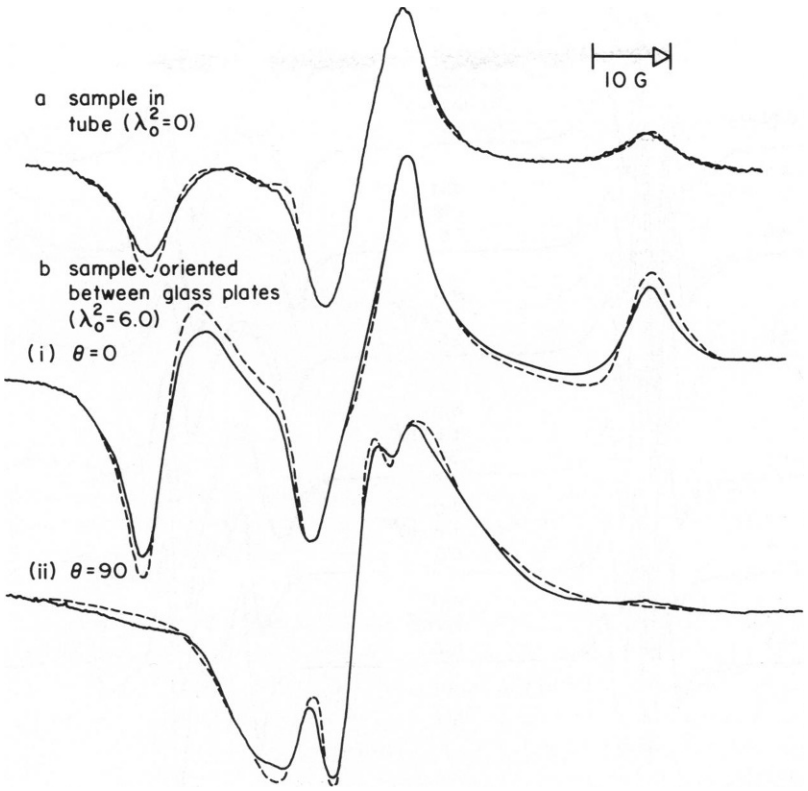

FIGURE 9 Experimental (solid line) and simulated (broken line) ESR spectra at $T = -150$°C for CSL in DPPC containing 2 wt % water. (*a*) Macroscopically disordered, sample in a tube, (*b*) sample oriented between plates and hence exhibiting both macroscopic and microscopic order. T_2^{*-1} used for simulations was 3.5 G in both *a* and *b*. Note that the linewidth at this temperature is too large for the second radical (Fig. 13) to be well resolved.

as $N = R_\parallel/R_\perp$. $T_2^{*,-1}$ denotes the inhomogeneously broadened linewidth.

Table II lists the ordering parameters (λ_0^2 and $\langle D_{00}^2 \rangle$) and diffusion rates ($R_\perp$ and $R_\parallel$) for CSL in DPPC for various temperatures. Several important points regarding the CSL spectra and their simulations are discussed below.

The Arrhenius type plot of τ_R vs. $1/T$ (Fig. 11) indicates two phase transitions above room temperature (22°C) in the DPPC-water system. The 16-PC spectra (Fig. 12 *b*) show these phase transitions more clearly than the CSL spectra (Figs. 10 and 12 *a*). Both transitions occur over a range of 5 to 10° within which a two phase region seems to exist. Simulations were not attempted for spectra from these two phase regions at the phase transitions. The gel to L_α phase transition, occurring at a low temperature, is the commonly reported phase transition for these low water-content DPPC systems. However, there are few references to the transition observed at a higher temperature. It is generally accepted that the liquid crystalline $L_\alpha(1)$ phase persists until the optically isotropic phase is observed at $T > 160$°C. In our low water-content DPPC samples the

TABLE I
MAGNETIC PARAMETERS*

Spin label	$A_{x'''}$	$A_{y'''}$	$A_{z'''}$	A_{iso} (experiment)‡	$A_{z'''}$ (experiment)§
	G	*G*	*G*	*G*	*G*
CSL‖	5.0	5.0	33.5	14.5 ± .1	33.6 ± .5
16-PC	6.5	6.5	30.0	14.3 ± .1	31.0 ± 1.0
8-PC	6.0	6.0	31.0	14.3 ± .1	32.0 ± 1.0
5-PC	5.0	5.0	33.0	14.3 ± .1	33.0 ± 1.0

*g used in all simulations ≡ g for CSL in cholestryl chloride, i.e., $g_{x'''} = 2.0089$, $g_{y'''} = 2.0056$, $g_{z'''} = 2.0021$.
‡Measured by heating the sample to the optically isotropic phase (also isotropic from the ESR point of view).
§Measured from rigid limit spectra at $T = -150$°C using tube samples.
‖For CSL in (DPPC + cholesterol) *A*: 4.8, 4.8, 34.5 G was used in the simulations.

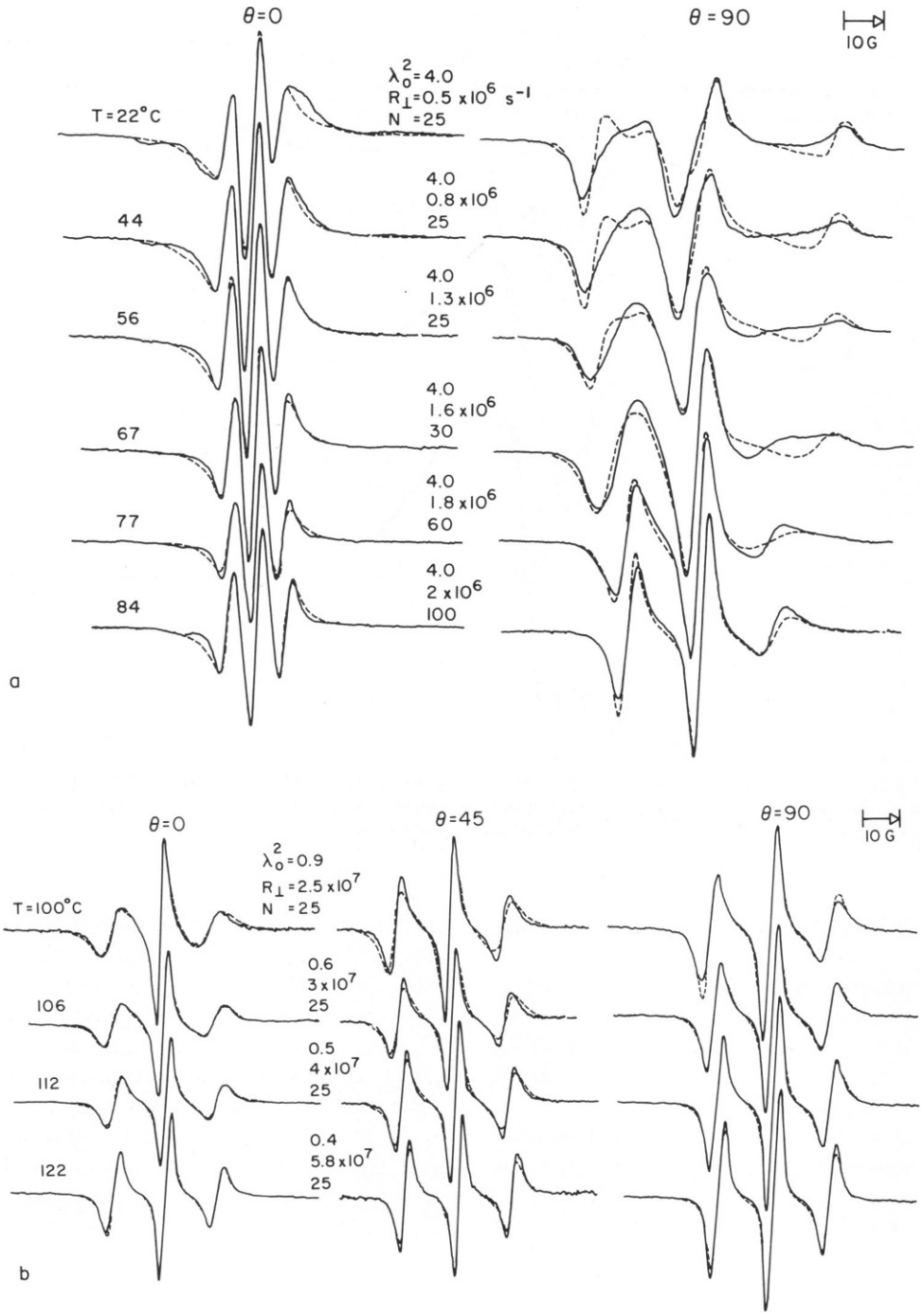

FIGURE 10 Experimental (solid line) and simulated (broken line) ESR spectra for oriented DPPC samples containing CSL and 4 wt % water. (*a*) Temperature-dependent spectra for the range 22°C ≤ T ≤ 84°C; (*b*) temperature dependent spectra for 100°C ≤ T ≤ 122°C.

$L_\alpha(1)$ phase appears to exist only for 10 to 20°. A high-temperature phase, referred to as F_2 (following Furuya and Mitsui [47]) occurs above the $L_\alpha(1)$ phase and persists up to the isotropic phase transition. Although the F_2 phase remains smectic A in nature, it is characterized by very low ordering compared with the $L_\alpha(1)$ phase. For DPPC in the presence of excess water, such a high-temperature phase, between the $L_\alpha(2)$ and isotropic, has been reported to occur at ~60°C (47). Structural implications regarding the F_2 phase are discussed in the section entitled Further Discussion.

For CSL the theoretical value of the anisotropy ratio N ($N = R_\parallel/R_\perp$) is 4.7, estimated using the dimensions of the molecule (5, 9, 48). Values of 4.7 and 5 have been used successfully by other workers for CSL in nematic and smectic phases (9–11, 30, 31). However, for CSL in DPPC, N has to be much larger than the predicted value of 4.7 for agreement between the experimental and simulated

TABLE II
PARAMETERS FOR MOLECULAR ORDERING AND ANISOTROPIC ROTATION OF CSL IN DPPC CONTAINING ~4 wt % WATER

Temperature	Phase	λ_0^2	$\langle D_{00}^2 \rangle$	$R_\perp$	$N = R_\parallel/R_\perp$	$\tau_R = (36\, R_\parallel R_\perp)^{-1/2}$	T_2^{*-1}	E_{act}
°C				s^{-1}		s	G	*Kcal/mol*
22		4.0	0.71	5×10^5	25	6.7×10^{-8}	1.6	
44	gel	4.0	0.71	8×10^5	25	4.2×10^{-8}	1.5	5
56		4.0	0.71	1.3×10^6	25	2.6×10^{-8}	1.3	
67	liquid	4.0	0.71	1.6×10^6	30	1.9×10^{-8}	1.0	
77	crystal	4.0	0.71	1.8×10^6	60	1.2×10^{-8}	1.0	12
84		4.0	0.71	2.0×10^6	100	8.3×10^{-9}	1.0	
100	liquid	0.9	0.20	2.5×10^7	25	1.3×10^{-9}	0.9	
106	crystal	0.6	0.13	3.0×10^7	25	1.1×10^{-9}	0.9	12
112	(F_2)	0.5	0.11	4.0×10^7	25	8.3×10^{-10}	0.9	
122		0.4	0.08	5.8×10^7	25	5.8×10^{-10}	0.9	

spectra. Even for the high temperature phase (corresponding to faster rotational diffusion rates) a minimum value of 15 is necessary for satisfactory fits between experiment and calculations. For the low-temperature phases this discrepancy between N (estimated) and N (required for best fit) becomes even larger (refer to Table II). Although the values of N in Table II may not reflect the true anisotropy in the rotational diffusion tensor, it is not unreasonable to assume that solvent-solute interactions change with structural changes in the different phases of the solvent. Part of the reason for this discrepancy may be the failure of our theoretical model to approximate the complicated physical situation as the ordering increases and motion decreases. In the motionally narrowed region it has been shown (6, 7) that an apparent N larger than that expected from the geometry of the probe molecule may be explained in terms of a slowly relaxing local structure (SRLS) model. Extrapolated to the low-temperature slow motional region, this may indicate that the CSL molecule experiences a local instantaneous ordering that is larger than the mean or equilibrium value of ordering $\langle D_{00}^2 \rangle$ estimated from the ESR analysis (10).

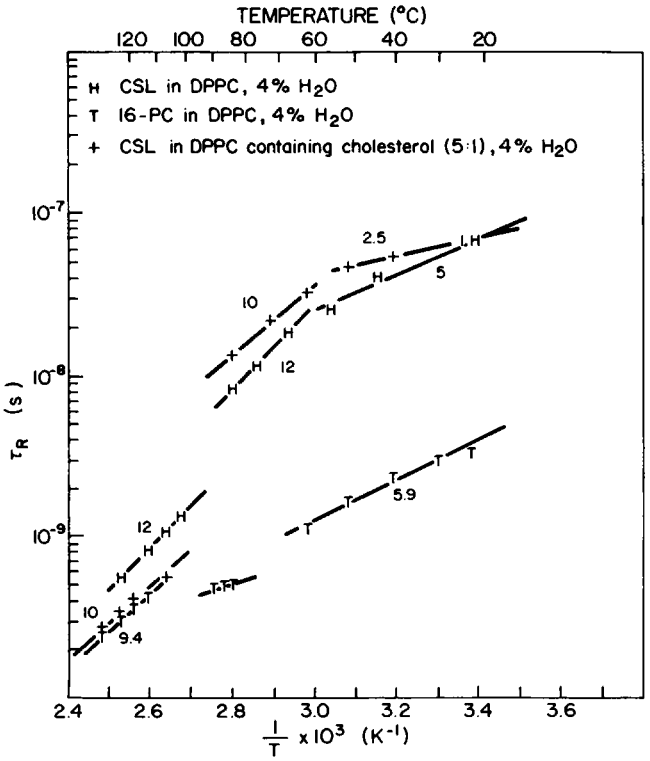

FIGURE 11 The Arrhenius type plots of τ_R vs. $1/T$. Activation energies calculated using these plots $\{\Delta E = R\,(\partial \ln \tau_R)/[\partial(1/T)]\}$ are shown next to the plots.

We were able to obtain only a fair fit for the spectra at low temperatures ($T < 60$°C), especially for $\theta = 90°$. Including higher order terms in the potential (like D_{00}^4) or introducing asymmetry in the ordering tensor by using a $\langle D_{02}^2 + D_{0\text{-}2}^2 \rangle$ term, did not improve the spectral fit in a significant way. Use of a diffusion model other than Brownian (e.g., the jump diffusion model similar to the one used by Dammers et al. [49] or the use of anisotropic viscosity) also did not have a significant effect. Simulations were also performed assuming a certain percentage of macroscopic disorder to be present in the microscopically ordered sample; i.e., a spectrum calculated using a particular model of director distribution was superimposed on a spectrum calculated assuming no distribution of directors to be present. The spectral resolution is not good enough to detect a contribution of <10% from macroscopic disorder. However, it is clear from Fig. 4 *c* that this sort of model, using ≥10% macroscopic disorder, does not fit the experimental spectra for well-oriented samples (Fig. 4 *b*).

At low temperatures ($T \leq 22$°C) a special feature is observed in the CSL spectra. Small shoulders are seen on the two outer lines, both for $\theta = 0°$ and $\theta = 90°$ (Fig. 13 *a*). At other angles the shoulders are not well resolved. These shoulders become better resolved as the temperature is lowered to the rigid limit (Fig. 13 *b*). They are also clearly visible in CSL spectra from DPPC multilayers containing cholesterol (Fig. 13 *c*). This feature has been observed

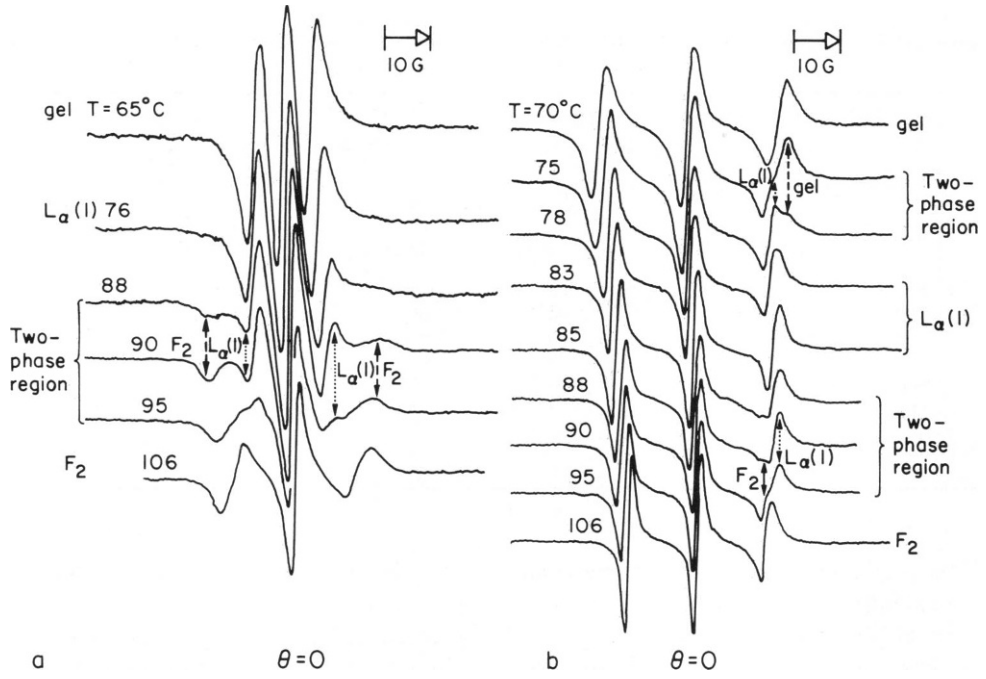

FIGURE 12 Experimental ESR spectra from oriented DPPC samples containing 2 wt % water and (*a*) CSL; (*b*) 16-PC as spin labels. The first phase transition above 22°C (gel to $L_\alpha[1]$) is observed around 75°C (note appearance of extra peaks in the spectra for 75°C and 78°C at the high field end in *b*). The second phase transition ($L_\alpha[1]$ to F_2) occurs around 90°C (note extra peaks in spectra for 88°C, 90°C and 95°C in both *a* and *b*.

before in ESR spectra of CSL from DPPC multilayers containing 25 mol % cholesterol (42). The spectra were recognized to be due to the superposition of two components corresponding to CSL molecules in two different environments in the sample. The smaller contribution (broad outer shoulders or peaks) was found to depend on sample preparation and hence was assumed to be from regions containing imperfect macroscopic ordering. Our simulations using a model of static distribution of directors do not support this macroscopic defect model. We have tried several different director distributions, e.g., (*a*) pure random, (*b*) Gaussian, (*c*) $\exp[C_2D^2_{00}(\theta) + C_4D^4_{00}(\theta)]$. We prefer a model in which the two environments (or sites) differ in nature (e.g., polarity) rather than macroscopic ordering. The following observations support our model.

(*a*) Peaks from unoriented regions (corresponding to random distribution of directors) occur at the outer extrema of the $\theta = 0°$ spectra (marked with solid arrows in Fig. 13). These peaks do depend upon sample preparation, they correlate with optical observation of macroscopic defects and are well simulated by superposition of a small random component (as shown in Fig. 4). However, there appears to be no correlation between the contributions from this type of macroscopic disorder and the second component giving rise to the shoulder described above (marked by broken arrows in Fig. 13), except that the shoulders are better resolved in defect free samples. Also, the PC probes do not show two component spectra at low temperatures.

(*b*) The lineshape is not affected by reducing the concentration of the spin probe from 5×10^{-3}M to 10^{-3}. This eliminates dipole-dipole interaction as a possible model.

(*c*) The correlation that is observed is one with water content of the pure DPPC multilayers. Contribution from the second component (marked with broken arrows in Fig. 13) increases with increase in water content of these samples (Fig. 13 *b*).

(*d*) Samples containing the PC probes do not show two component spectra at low temperatures, implying that the location of the nitroxide group within the bilayer is important for detecting the second component.

(*e*) Simulations using different tensors to describe the hyperfine interactions for the two components (I and II in Fig. 13) fit the experimental spectra fairly well. The components of the hyperfine tensors A_I and A_{II} are different, with A_{II} having a larger trace than A_I, as expected for a more polar environment. However, $TrA_{II} \simeq$ 19.7 G obtained from simulation is larger than $TrA \simeq 16$ G for CSL in polar solvents (9). This may be due to structural differences in the polar site possibly due to packing of the highly ordered DPPC multilayers at low temperatures, which may distort the nitroxide moiety. Such large magnetic parameters have been reported before for other nitroxides in oriented media (8, 30, 31). In fact, a trace of 19.05 G has been reported for the stearamide probe in the $L_\alpha(1)$ phase of oriented lipid samples (31), the same probe giving a trace of 16.2 G in lipid samples contained in a

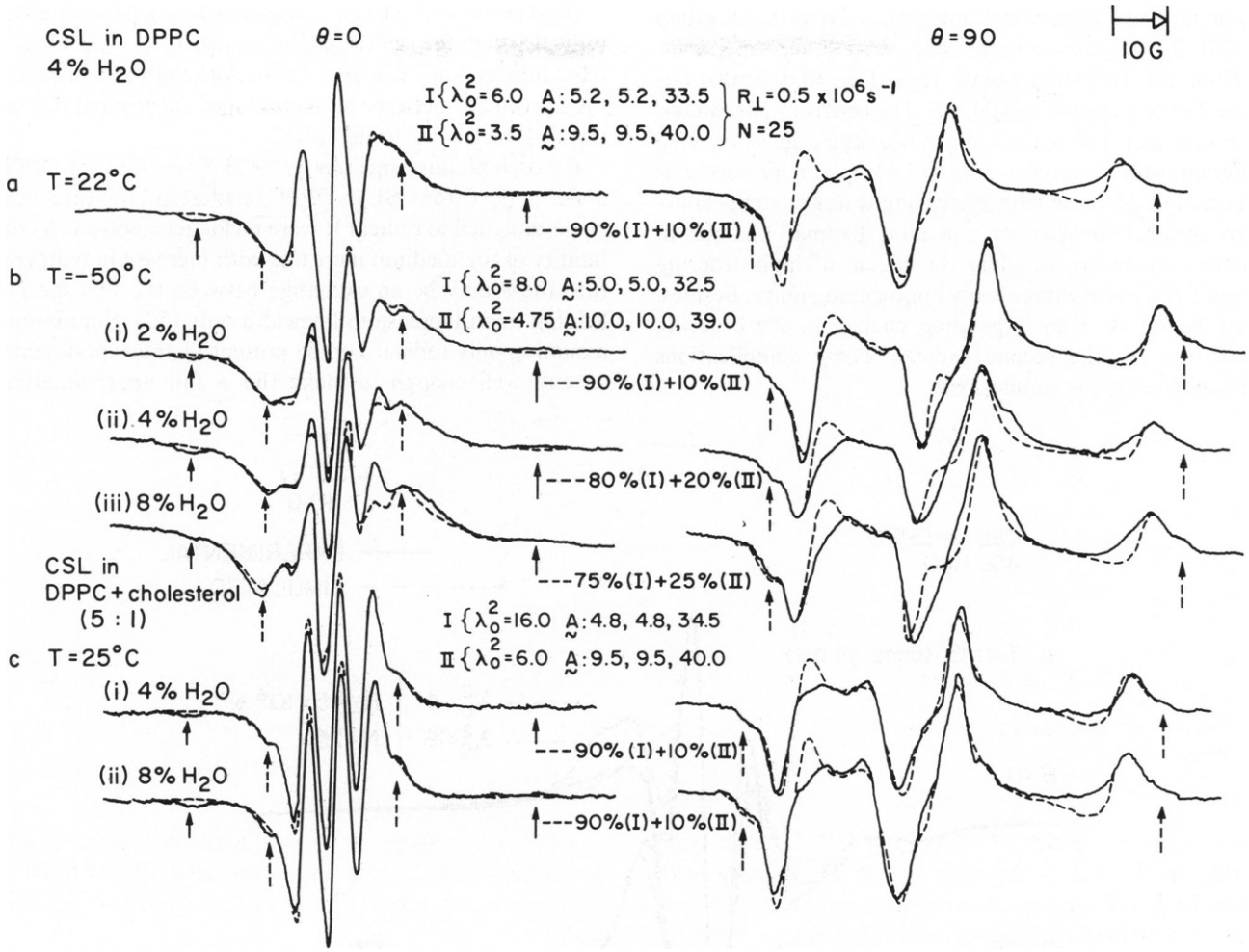

FIGURE 13 Experimental (solid line) and simulated (broken line) ESR spectra indicating the presence of a second radical, detectable at low temperatures. Positions of peaks due to macroscopic disorder present in the sample are marked with solid arrows. Spectral contributions from the second radical are marked with broken arrows. (*a*) Spectrum at T = 22°C for CSL in DPPC containing 4 wt % water; (*b*) spectrum at T = −50°C for CSL in DPPC containing (*i*) 2 wt %, (*ii*) 4 wt %, (*iii*) 8 wt % water; (*c*) spectrum at T = 25°C for CSL in DPPC containing cholestrol (DPPC/cholesterol = 5:1) and (*i*) 4 wt %, (*ii*) 8 wt % water.

tube. As suggested in that work (31) strong cooperative interbilayer forces may be present in the headgroup regions of oriented multilayer samples, distorting the nitroxide moiety and thereby affecting its magnetic parameters. The biaxial nature of the gel phase (33–35) is indicative of such cooperative forces.

Two possible explanations for these two component spectra are discussed below. (*i*) Radical II corresponds to a CSL molecule in which the nitroxide is hydrogen bonded to a water molecule. A similar spectral observation and explanation has been reported for PD-tempone in ethanol-d_6 (5). Increase in water content then would increase the number of hydrogen bonded species.

(*ii*) A phase separation occurs at low temperatures in these DPPC-water systems, resulting in two distinct regions with different water contents. Then A_I might correspond to the region with low water content (say a monohydrate, i.e., 2% by weight water), while A_{II} would refer to the higher water content region. Evidence of complex polymorphic behavior, involving a metastable dehydrated crystal form and a stable hydrated crystal form has been observed in hydrated lipids below the liquid-crystalline L_α phase (50, 51). Although similar evidence is not available for partially hydrated (low water content) lipids such a model appears plausible.

However, our observations using the DPPC samples containing cholesterol lead us to prefer explanation *i*. ESR spectra from these samples do not show an increase in component II with increase in water content (Fig. 13). This seems consistent with the hydrogen bonding model since in the presence of cholesterol, CSL would have to compete with the cholesterol molecules for water available for hydrogen bonding. Hence a small increase in water may not reflect any corresponding increase in hydrogen bonded CSL or species II. However, considering the uncertainties in the water content of our samples, and the possibility that phase separation may be altered in the presence of cholesterol, we cannot rule out the second explanation. We would

like to note that both models imply that the nitroxide group in CSL is located close to the lipid-water interface.

Note the following points regarding the simulations using the two species model. (*a*) The ordering parameter, λ_0^2, was assumed to be the same in the simulations involving different water contents (Fig. 13 *b* and *c*). Ordering is expected to decrease with increasing water content. However, spectral changes corresponding to small changes in ordering alone are small in the region of high ordering where $\langle D_{00}^2 \rangle$ is asymptotically approaching unity. Besides, there would be a corresponding change in the ordering parameter for the second radical. These complications were avoided in the simulations.

(*b*) The simulations use a higher ordering parameter for radical I than for radical II (for example, at -50°C, λ_I = 8.0 while λ_{II} = 4.75 in Fig. 13 *b*). Although this improves the agreement between simulated and experimental spectra, it is not crucial to the model.

(*c*) At high temperatures ($T \geq 23$°C for CSL in DPPC and $T \geq 60$°C for CSL in DPPC/cholesterol mixtures) the peaks assigned to radical II were no longer resolved. As the fluidity of the medium increases with increase in temperature there may be an exchange between the two species, leading to an increase in linewidth only (52). Simulations assuming only radical I to be present fit the experimental spectra well enough to make this a fair approximation.

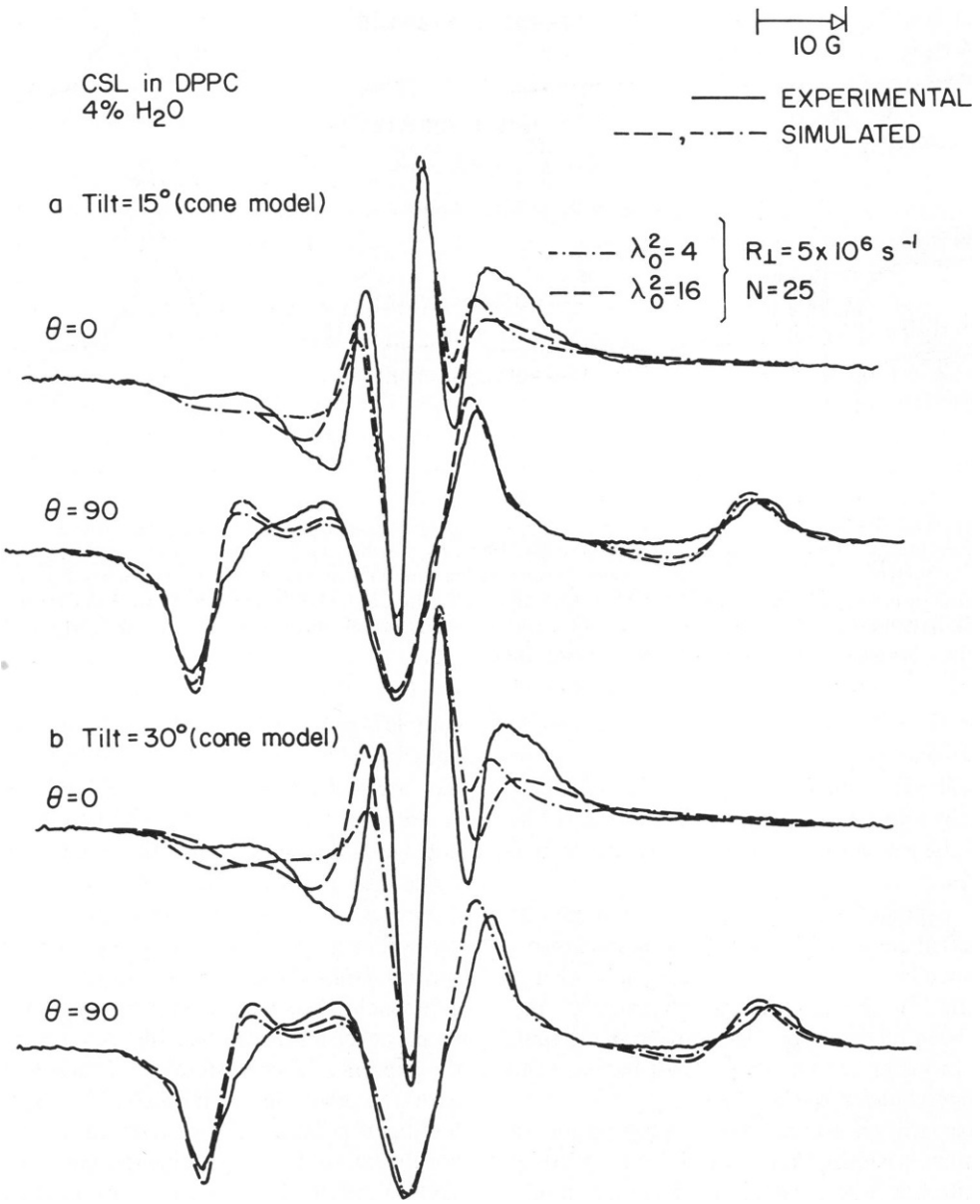

FIGURE 14 Attempt to simulate the ESR spectra at low temperature (T = 22°C) using the cone model of director tilt (see text). (*a*) Tilt = 15° (C_2 = 7.5, C_4 = −2.5); (*b*) tilt = 30° (C_2 = 10, C_4 = −5). Although there is a slight improvement in the fit for θ = 90° spectra, it is insignificant compared with the poor fit for θ = 0° spectra, showing that such a director tilt model does not fit the data for CSL in DPPC.

Alternatively, the configuration of CSL molecules within the bilayer may change slightly with increase in temperature, making hydrogen bonding less favorable.

Molecular Tilt. X-ray diffraction studies of both unoriented (14) and oriented (15) phospholipid multilayers give evidence of hydrocarbon chain tilt in the gel phase. It is generally accepted that the degree of tilt depends on the degree of hydration of the phospholipid multilayers. For fully hydrated DPPC this tilt is estimated to be ~33° (53). For low water content DPPC (<10% water by weight) chain tilt was previously assumed to be negligible (15). More recent x-ray diffraction data (54), however, seem to indicate a 12.5° tilt for ~10% by weight water. For single crystals of DPPC containing less water than the monohydrate (i.e., <2.5% water by weight), Asher et al. (22) have estimated a tilt of 25° to 30°, which appears to contribute to the large birefringence observed. For aligned DPPC samples with ~11% water, Hemminga (42) estimates a tilt of ~23° (for $T < 0$°C) from ESR studies.

In our experiments using CSL, the smectic A nature of the ESR spectra is maintained even at low temperatures ($T < 0$°C); i.e., the spectrum at θ_n is identical with the spectrum at $\pi - \theta_n$ (or $-\theta_n$) where θ_n is the angle between the plate normal and the external magnetic field. For a purely smectic C type director tilt of angle β (with respect to the plate normal) symmetry would be observed about $\theta_n = \beta$ (or $\theta_n = \beta + \pi/2$) instead of about $\theta_n = 0$ (or $\theta_n = \pi/2$) as in our experiments. However, if the smectic C director had a random component in the xy plane (i.e., in the bilayer plane) the ESR spectra would still show the observed smectic A symmetry about $\theta_n = 0$ (or $\theta_n = \pi/2$). We refer to this model as the cone model since there is now a static distribution of directors lying on a cone of solid angle 2β. We can simulate spectra using this model by convolution of spectra corresponding to all director tilts (0° to 90°) with a distribution function of the form $P(\theta) \propto \exp [C_2 D^2_{00}(\theta) + C_4 D^4_{00}(\theta)]$. While the coefficient C_2 affects the width of the distribution, the ratio C_2/C_4 affects the positions of the extrema as a function of θ. By proper choice of values for these coefficients we have simulated spectra corresponding to $\beta = 15$° and $\beta = 30$° in the cone model (i.e., the maxima of the resulting distribution functions occur at ±15° and ±30°). Comparison with experimental CSL spectra shows that these cone models do not fit our data from CSL (Fig. 14).

The spectra we obtained at low temperatures ($T <$ 22°C) using CSL in pure DPPC-water samples are quite different in appearance from the rigid-limitlike spectra reported by Hemminga (42) for similar systems. The difference (a chain tilt of ~23° estimated by Hemminga) may be due to the lower water content of our samples or due to differences in our sample preparation techniques. Differentials of this type should be always kept in mind when different studies are intercompared (e.g., this study and references 42–44).

In the case of 16-PC, however, a new feature is observed in the ESR spectra for sample temperatures below 22°C. Since the PC probes are z ordered (Fig. 6), the spectrum at $\theta = 0$ has the largest spectral width (or $\langle 2a \rangle_{\theta=0} = \langle 2a \rangle_{max}$, where θ describes the director tilt). For $T > 22$°C the maximum spectral width is observed at $\theta_n = 0$, implying that the director is aligned approximately parallel to the plate normal. However, for $T \leq 22$°C, the maximum spectral width occurs at θ_n values of 35° to 45° indicating a nonzero director tilt. Fig. 15 a shows this feature for 16-PC in DPPC at $T = -75$°C. Rigid limit simulations for orientation-dependent spectra give a reasonable fit only when a director tilt of ~30° is assumed (Fig. 16 *b*[*i*]). To be consistent with our sample preparation technique this tilt cannot be a pure smectic C-type tilt, but rather a cone-type tilt as explained earlier. In the absence of director tilt of any kind, the fit is poor at all angles (Fig.

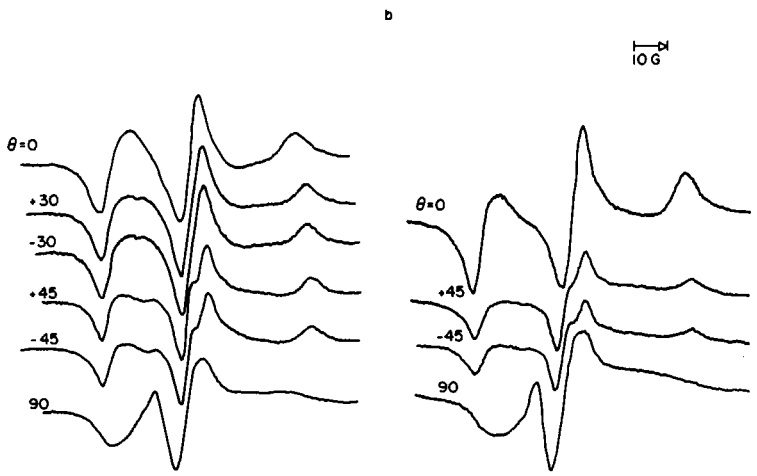

FIGURE 15 Experimental ESR spectra indicating director tilt. (*a*) Spectra for 16-PC in DPPC at −75°C; (*b*) Spectra for 5-PC in DPPC at 24°C. Note that in both *a* and *b* $\langle 2a \rangle$ at $\theta = 0° < \langle 2a \rangle$ at $\theta = 45°$.

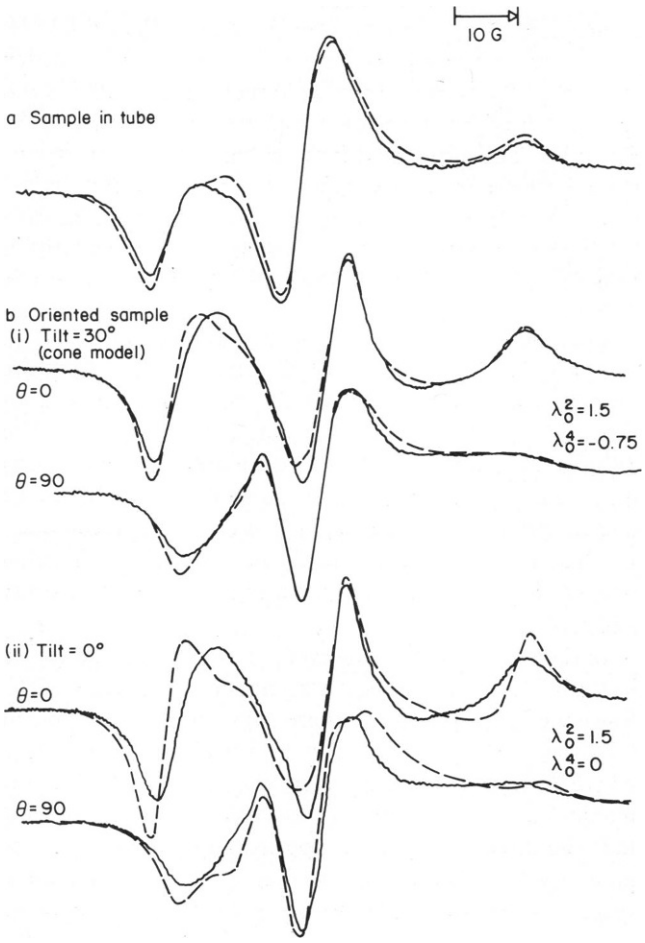

FIGURE 16 Experimental (solid line) and simulated (broken line) ESR spectra in the rigid limit (at $T = -75$°C) for 16-PC in DPPC containing 4 wt % water. (*a*) Spectrum from sample in a tube (i.e., with no macroscopic ordering). Simulation assumes a random distribution of directors (corresponding to $\lambda_0^2 = 0 = \langle D_{00}^2 \rangle$ in the rigid limit). (*b*) Spectrum from sample oriented between plates. Simulations assume presence of macroscopic ordering with $\lambda_0^2 = 1.5$ ($\langle D_{00}^2 \rangle = 0.34$). Simulations in *i* assume a cone model for director tilt, with tilt angle $\beta = 30°$. Simulations in *ii* assume director tilt to be zero. Simulations in *i* give a better fit for both $\theta = 0°$ and 90°.

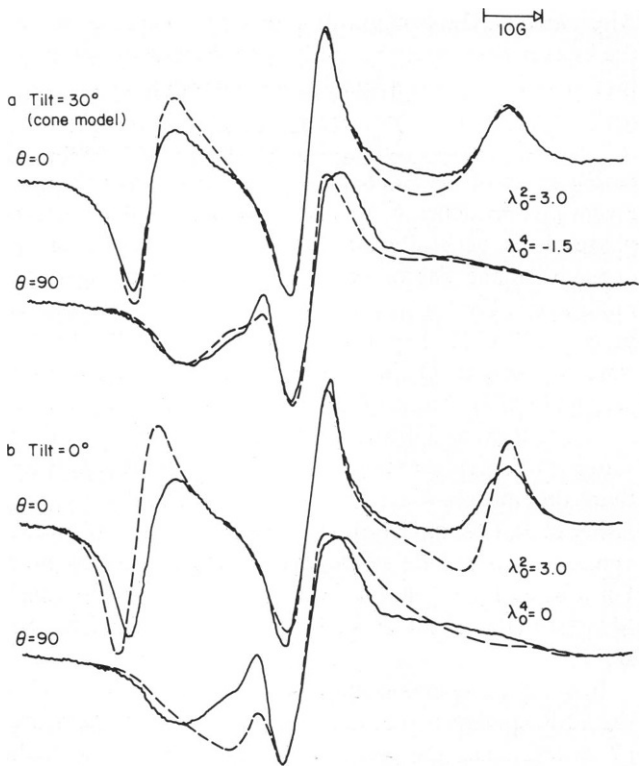

FIGURE 17 Experimental and simulated ESR spectra in the rigid limit (at $T = -75$°C) for 5-PC in DPPC containing 4 wt % water. Simulations in *a* assume a 30° tilt (cone model) while those in *b* assume absence of director tilt. Macroscopic ordering is assumed in both *a* and *b*, with $\lambda_0^2 = 3.0$ ($\langle D_{00}^2 \rangle = 0.60$). Intrinsic linewidth ($T_2^{*-1}$) = 4.0 G.

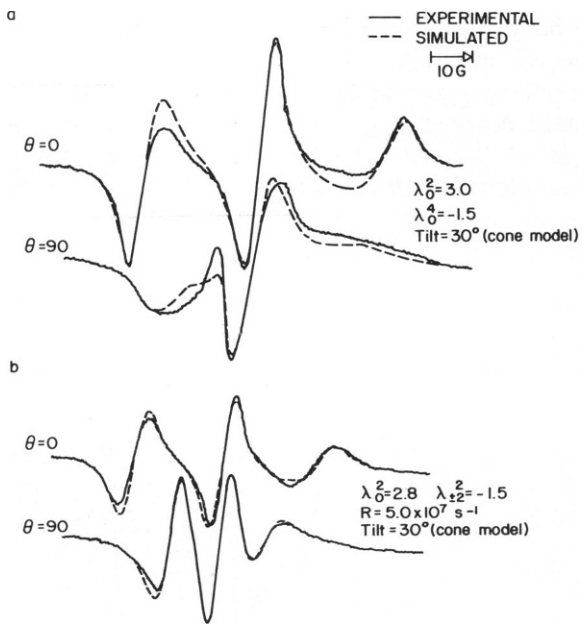

FIGURE 18 Experimental and simulated ESR spectra for 5-PC in DPPC at $T = 24$°C. Simulations are as for Fig. 17 *a*, except $T_2^{*-1} = 3.5$ G. (*b*) Experimental and simulated spectra for 16-PC in DPPC at $T = 30$°C. Simulations assume an asymmetric potential ($\lambda_{\pm 2}^2 = -1.5$) and a static director distribution in a cone of half angle $\beta = 30°$, the distribution having a halfwidth = 15°.

14 *b*[*ii*]). (The fit [using tilt = 0°] may be improved to some extent by adjusting the A tensor. However, the A tensor is then not consistent with that estimated from the rigid limit spectrum from a tube sample, where models of director tilt and ordering do not complicate the picture [Fig. 16 *a*]). This idea of a cone model for director tilt may be carried through in a similar fashion for 5-PC in DPPC. At rigid limit a cone model for director tilt, with tilt angle $\beta \simeq 30°$ fits the data better than a model assuming absence of director tilt (Figs. 17 *a*, *b*). In fact, for 5-PC an indication of director tilt is obtained at $T = 24$°C (i.e., $\langle 2a \rangle_{\theta=0} < \langle 2a \rangle_{\theta=45}$ at $T = 24$°C; Fig. 15 *b*). The location of the nitroxide in 5-PC being close to the head group, the molecular rotational reorientation rate for 5-PC is expected to be much slower in comparison to that of 16-PC, which monitors the more flexible hydrocarbon tail

region. Comparison of spectra at $T = 24°C$ (Fig. 18 *a*) with spectra at $T = -75°C$ for 5-PC in DPPC (Fig. 17) shows that the rotational diffusion rate for 5-PC is close to the ESR rigid limit at $T = 24°C$. In fact, the rigid limit simulations assuming a cone model with tilt = 30° (similar to Fig. 17 *a*) fit the spectra corresponding to $T = 24°C$ fairly well (Fig. 18 *a*). A small reduction of the intrinsic linewidth parameter, T_2^{*-1}, from 4.0 G at −75°C to 3.5 G at 24°C is required; but this is not unreasonable considering the temperature dependence of inhomogeneous broadening for such nitroxide labels.

The 5-PC spectra then point out that the director tilt may be present even at higher temperatures, although spectral features do not make this directly evident until the molecular rotational diffusion rate has slowed down sufficiently. In other words, the director, or hydrocarbon chain tilt may be present throughout the gel phase (even at higher temperatures) and need not be a structural alteration that occurs at lower temperatures ($T < 22°C$) only. At higher temperatures, the faster molecular reorientation rates would mask the spectral features first noticed as evidence of tilt (i.e., $\langle 2a \rangle_{\theta=0°} < \langle 2a \rangle_{\gamma}$ for $\gamma = 30°$ or 45°). However, agreement between simulated and experimental spectra is improved when a cone model of director tilt is used. Fig. 19 *a* and *b* illustrate this observation at $T = 65°C$ for 5-PC and 8-PC, respectively, in DPPC. For 16-PC the rotational diffusion rate is high enough so that simulations are less model sensitive. Therefore, for the high T end of the gel phase, agreement between simulated and experimental spectra are fairly good even with a model assuming absence of director tilt (Fig. 20 *a*, $T = 63, 52°C$). The agreement is not so good at the lower temperatures (Fig. 20*a*, $T < 41°C$). That the director tilt model fits the spectra better for these low temperatures is illustrated in Fig. 18 *b*. The agreement between simulated and experimental spectra is greatly improved for the $\theta = 90°$ case at $T = 30°C$. Note that the simulation parameters do need to be altered when director tilt is assumed in the calculations. Usually ordering (described by λ_0^2 or $\langle D_{00}^2 \rangle$ etc.) needs to be increased or motion (R) needs to be decreased or both in the simulation using director tilt (compare parameters in Figs. 18 *b* and 20 *a* for 16-PC in DPPC at $T = 30°C$).

Therefore, although no molecular tilt was indicated by CSL, there appears to be a fair amount of evidence from all three labeled PC probes that even for low water-content DPPC the hydrocarbon chains may be tilted away from the bilayer normal by as much as 30° in the gel phase of these oriented multilayers. The nitroxide on CSL may be located too far into the lipid-water interface to be a useful or accurate probe of hydrocarbon chain conformation. Our observation suggesting that the nitroxide on CSL may take part in hydrogen bonding with water molecules, seems consistent with this idea.

Effect of Addition of Cholesterol. Fig. 21 shows the experimental and simulated spectra obtained at $T = 25°C$ using CSL in oriented multilayers of DPPC containing various concentrations of cholesterol. At 1:40 concentration of cholesterol to DPPC the spectra are virtually identical with those from pure DPPC multilayers with the

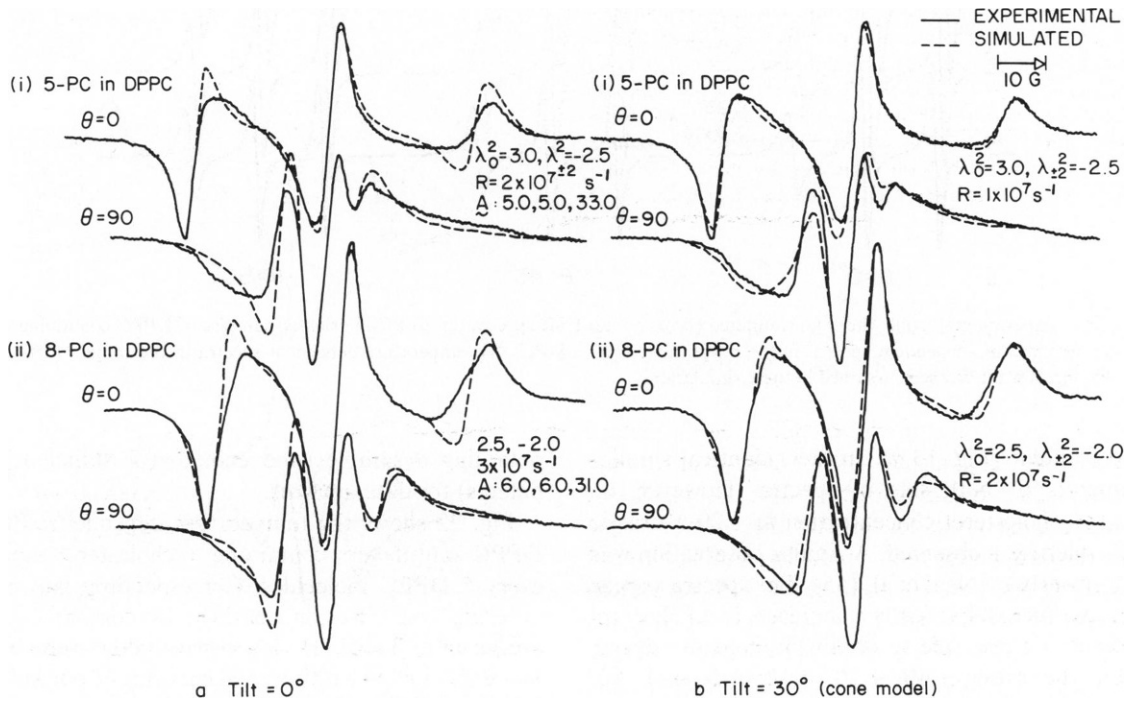

FIGURE 19 Experimental and simulated ESR spectra at $T = 65°C$ for (*i*) 5-PC in DPPC, (*ii*) 8-PC in DPPC. Simulations in *a* for both *i* and *ii* assume director tilt = 0°. Simulations in *b* assume a cone model for director tilt, with tilt ≃30° (halfwidth of the distribution function used ≃ 15°). Note that the rotational diffusion rate had to be reduced for better fits in *b*.

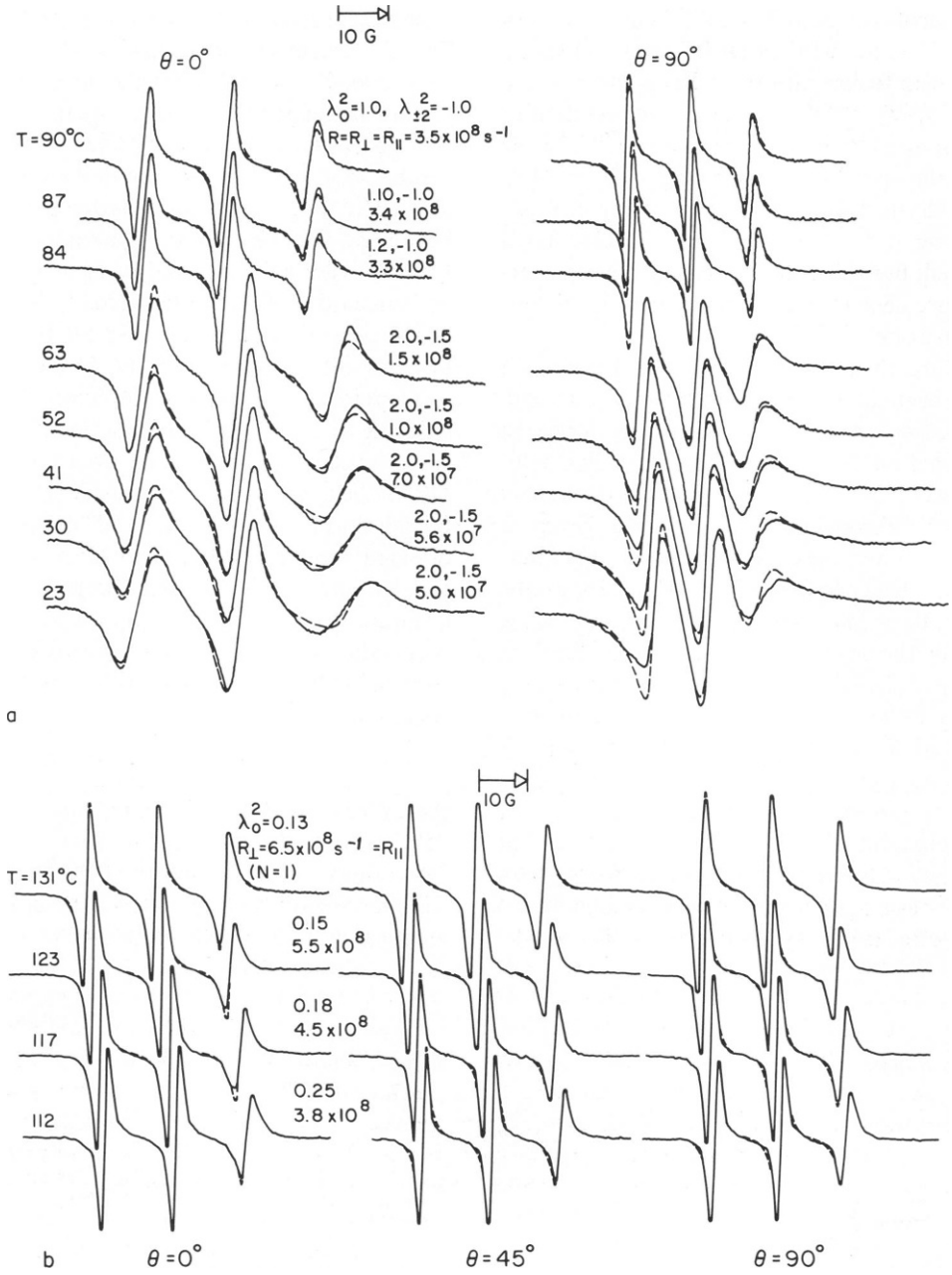

FIGURE 20 Experimental (solid line) and simulated (broken line) ESR spectra for 16-PC in oriented samples of DPPC containing 4 wt % water. (*a*) temperature-dependent spectra in the range 23°C < T < 90°C; (*b*) temperature-dependent spectra in the range 112°C < T < 131°C. No director tilt has been assumed in these simulations.

same water content (Fig. 13 *a*). In fact, identical simulation parameters fit both sets of spectra. However, on increasing the cholesterol concentration to 1:20 a drastic increase in ordering is observed. A similar observation was reported previously by Neal et al. (55). The spectra appear to remain unaffected by further increase in cholesterol concentration. We are able to obtain ordered multilayer samples for the ratios 1:40, 1:20, 1:10, 1:5, and 1:2. However, as the cholesterol concentration was increased it became more and more difficult to obtain defect free samples. In fact, for the 1:2 ratio we were not successful in obtaining a sample good enough (or sufficiently free of defects) for data analysis.

Fig. 22 shows the temperature dependence of oriented DPPC multilayers containing 1 cholesterol molecule for every 5 DPPC molecules. Corresponding parameters for ordering and diffusion obtained by computer simulation are given in Table III. These parameters remain more or less unchanged (within the accuracies of our simulations) for the other cholesterol concentrations used (1:20 and 1:10). Comparison with Table II shows that although the ordering remains consistently high for multilayers contain-

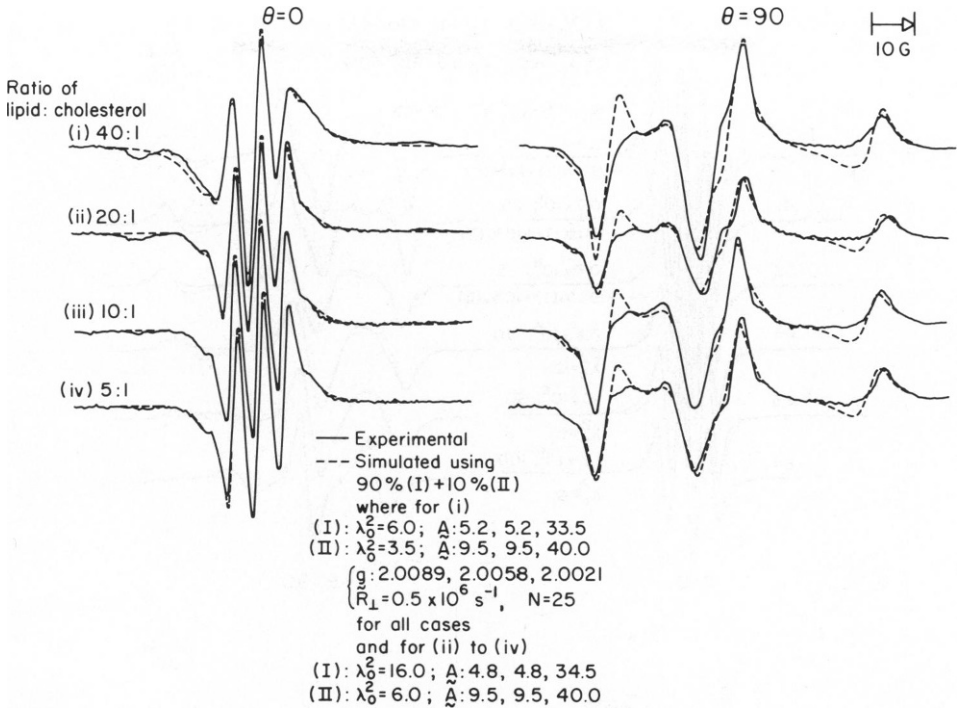

FIGURE 21 Experimental (solid line) and simulated (broken line) ESR spectra at T = 25°C for CSL in oriented samples of DPPC containing 4 wt % water and varying concentrations of cholesterol. The DPPC to cholesterol ratios are (*i*) 40:1, (*ii*) 20:1, (*iii*) 10:1, and (*iv*) 5:1. Simulations assume the presence of a second radical (II) with a larger $A_{isotropic}$ (A_{II}), as in Fig. 13. See text for discussion.

ing cholesterol, diffusion parameters ($R_\perp$, $R_\parallel$) are not significantly affected by cholesterol and remain within a factor of 2. The change of these parameters with temperature follows the same trend as the pure DPPC-water multilayers. The phase transition temperatures remain within 5° of the pure DPPC samples. As with the pure samples, the F_2 phase is obtained at high temperatures (Figs. 11 and 22*b*) and a second species (radical II) becomes resolved at low temperatures ($T \leq 60$°C in Fig. 22 *a*). Therefore, apart from the increase in ordering, these cholesterol containing multilayers behave very much like pure DPPC-water multilayers.

Considering that the lipid-water interface is known to be the anchoring site for cholesterol (56, 57) and the nitroxide group on CSL is also located close to the interface (as shown earlier in this section), one might expect CSL to be very sensitive to any changes in the bilayer brought about by the presence of cholesterol. However, CSL shows no effects on the bilayer structure and dynamics at a cholesterol concentration of 1:40. It is possible that at DPPC to cholesterol ratios smaller than 1:20, structural changes occur in the hydrocarbon chain region without changing the structure of the polar headgroup region (58), and the nitroxide on CSL is a poor probe for detecting small distortions in the hydrocarbon chain. Within the sensitivity obtainable using such spin labels as a probe of molecular structure and dynamics, a steplike concentration-dependent phase diagram may be proposed. (*a*) A certain number of cholesterol molecules (<1 for 20 DPPC molecules) may be incorporated into the bilayer without significantly affecting the bilayer structure; (a similar assumption is made regarding the probe molecule itself although at a much lower concentration of 1:200); (*b*) a threshold concentration exists corresponding to which a structural change must occur in the bilayer in order to accommodate more cholesterol molecules; (*c*) the new structure of the bilayer is such that it can accommodate more cholesterol molecules without further change (until a concentration is reached at which bilayer structure is no longer supported, which occurs at >1:2 concentration, i.e., for 1:1). The presence of cholesterol and the subsequent alteration in bilayer organization does not seem to affect the rotational diffusion rates of the CSL probe significantly, implying that the local microviscosity remains more or less unchanged. An increase in fluidity has been reported before (38). We observe a slight decrease in the rotational diffusion rates for $T < 100$°C. Our observations agree with recent studies using fluorescence spectroscopy (59), which showed that the major effect of cholesterol is to increase structural order in DPPC vesicles.

We considered CSL most appropriate for studying the effects of cholesterol on DPPC-water multilayers since it is known from previous studies (32, 38, 55–57 and references therein) that (*a*) the hydroxyl group of cholesterol is located close to the carbonyl group of the phospholipid, (*b*) the long axis of cholesterol aligns itself parallel to the lipid alkyl chains, extending ~11 Å into the hydrophobic region, (*c*) cholesterol tends to preserve the molecular order near

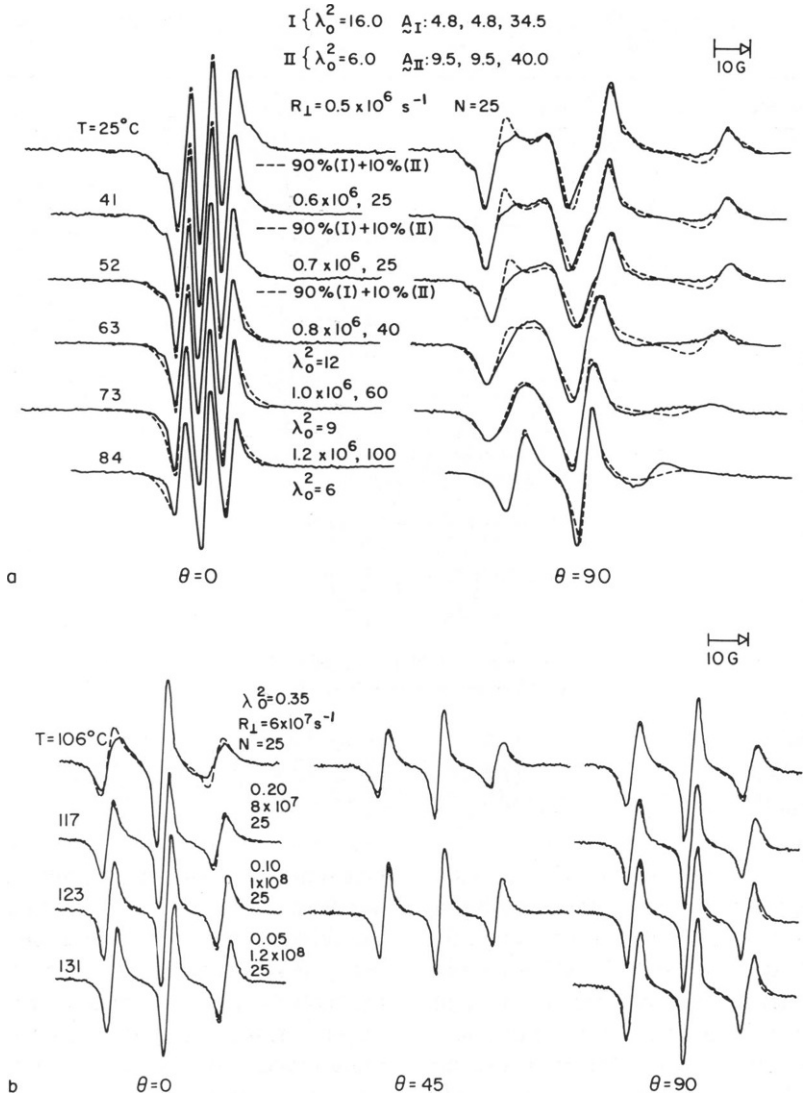

FIGURE 22 Experimental (solid line) and simulated (broken line) spectra for CSL in oriented DPPC multilayers containing cholesterol (DPPC/cholesterol = 5:1) and 4 wt % water. (*a*) Temperature-dependent spectra in the range 25°C < T < 84°C; (*b*) temperature-dependent spectra in the range 106°C < T < 131°C.

TABLE III

PARAMETERS FOR MOLECULAR ORDERING AND ANISOTROPIC ROTATION OF CSL IN DPPC + CHOLESTEROL (5:1) CONTAINING ~4 wt % WATER

Temperature	Phase	λ_0^2‡	$\langle D_{00}^2 \rangle$	$R_\perp$	$N = R_\parallel/R_\perp$	$\tau_R = (36\, R_\parallel R_\perp)^{-1/2}$	T_2^{*-1}	E_{act}
°C				s^{-1}		s	G	*Kcal/mol*
25		16	0.94	5.0×10^5	25	6.7×10^{-8}	1.7	
41	gel	16	0.94	6.0×10^5	25	5.6×10^{-8}	1.5	2.5
52		16	0.94	7.0×10^5	25	4.8×10^{-8}	1.5	
63	liquid	12	0.91	8.0×10^5	40	3.3×10^{-8}	1.5	
73	crystal	9	0.88	1.0×10^6	60	2.2×10^{-8}	1.5	10
84		6	0.82	1.2×10^6	100	1.4×10^{-8}	1.3	
106	liquid	0.35	0.07	6.0×10^7	25	5.6×10^{-10}	0.7	
117	crystal	0.20	0.04	8.0×10^7	25	4.2×10^{-10}	0.7	10
123	(F_2)	0.10	0.02	1.0×10^8	25	3.3×10^{-10}	0.7	
131		0.05	0.01	1.2×10^8	25	2.7×10^{-10}	0.7	

‡For T = 25, 41, and 52°C where a two-radical model was assumed in the simulations, λ_0^2 corresponding to only the predominant species has been tabulated (see Fig. 20 *a*).

TABLE IV
PARAMETERS* FOR MOLECULAR ORDERING AND ROTATIONAL REORIENTATION OF 16-PC IN DPPC CONTAINING ~4 wt % WATER

Temperature	Phase	λ_0^2	$\langle D_{00}^2 \rangle$	$\lambda_{\pm 2}^2$	$\langle D_{00}^2 + D_{0-2}^2 \rangle$	R§	$\tau_R = 1/6R$	T_2^{*-1}	E_{act}
°C						s^{-1}	s	G	*Kcal/mol*
23‡		2.0	0.38	−1.5	−0.27	5.0×10^7	3.3×10^{-9}	2.0	
30	gel	2.0	0.38	−1.5	−0.27	5.6×10^7	3.0×10^{-9}	2.0	5.9
41		2.0	0.38	−1.5	−0.27	7.0×10^7	2.4×10^{-9}	2.0	
52		2.0	0.38	−1.5	−0.27	1.0×10^8	1.7×10^{-9}	2.0	
63		2.0	0.38	−1.5	−0.27	1.5×10^8	1.1×10^{-9}	2.0	
84	liquid	1.2	0.21	−1.0	−0.26	3.3×10^8	5.1×10^{-10}	1.0	
87	crystal	1.1	0.19	−1.0	−0.27	3.4×10^8	4.9×10^{-10}	1.0	(4.0)‖
90		1.0	0.16	−1.0	−0.28	3.5×10^8	4.8×10^{-10}	1.0	
112	liquid	0.25	0.041	0**	0**	3.8×10^8	4.4×10^{-10}	0.8	
117	crystal	0.18	0.037	0	0	4.5×10^8	3.7×10^{-10}	0.8	9.4
123	(F_2)	0.15	0.031	0	0	5.5×10^8	3.0×10^{-10}	0.8	
131		0.13	0.026	0	0	6.5×10^8	2.6×10^{-10}	0.8	

*Parameters are from simulations assuming no director tilt.
‡See Fig. 18 b for changes in these parameters when a cone model of director tilt, with tilt = 30°, is considered.
§For the labeled PC probes (16-PC, 8-PC, and 5-PC) the simulations were not very sensitive to $N = R_\parallel/R_\perp$. Therefore a model of isotropic Brownian rotational reorientation was assumed (with $N = 1$).
‖Activation energy calculation was not considered to be accurate for this phase since data available for a temperature range of only 6°C.
**No asymmetry was assumed in the F_2 phase ($\lambda_{\pm 2}^2 = 0$) since simulations corresponding to such low ordering and high motion are generally insensitive to such details in molecular models.

the headgroup region (up to C_{12}) while allowing disorder to exist near the center of the bilayer (beyond C_{12}). Although 5-PC and 8-PC would probably show similar increase in ordering due to cholesterol, the length of the CSL molecule (approximately that of cholesterol) may make it a more suitable probe. 16-PC, on the other hand, would show little effect if any. (Note here that in a previous ESR study using egg-lecithin [60] a maximal response to added cholesterol for 12-PC and weaker responses for 5-, 7-, and 16-PC were reported). However in view of point (*c*) it would be interesting to study samples of higher water content (>20% by weight), using CSL to monitor cholesterol-mediated increase in ordering near the head group and 16-PC to show disorder near the tail, unaffected by addition of cholesterol.

Studies Using the PC Probes

Fig. 20 shows experimental and simulated spectra for 16-PC in DPPC-water multilayers. Table IV lists the parameters required for best fit of simulated spectra at various temperatures. Comparison with CSL parameters (Table II) shows that the ordering is lower while the rotational diffusion rate of 16-PC is higher. This is consistent with the expected increase in disorder and flexibility at the center of the hydrophobic region. Table V compares the simulation parameters for a particular temperature for the three PC probes studied. Our results agree with several previous results (60 and references therein) showing that ordering decreases from the hydrophilic headgroup region towards the hydrophobic center of the bilayer and this is accompanied by an increase in chain flexibility.

More spectacular than the change in ordering is the change in rotational reorientation rate (R) as one moves from the head to the tail region. R for 16-PC at 63°C is more than an order of magnitude higher than that for 5-PC at 65°C (see Table V), while R for 8-PC is only about a factor of 2 higher than that for 5-PC.

One important difference between CSL and the labeled PC probes is that a cylindrically symmetric potential

TABLE V
COMPARISON OF MOLECULAR ORDERING AND ROTATIONAL REORIENTATION PARAMETERS FOR 5-PC, 8-PC, AND 16-PC IN DPPC CONTAINING ~4 wt % WATER AT $T \simeq 65$°C

Spin label	Phase	λ_0^2	$\langle D_{00}^2 \rangle$	$\lambda_{\pm 2}^2$	$\langle D_{02}^2 + D_{0-2}^2 \rangle$	R	$\tau_R = 1/6R$	T_2^{*-1}
						s	s	G
5-PC	gel	3.0	0.42	−2.5	−0.30	1.0×10^7	1.7×10^{-8}	1.8
8-PC	gel	2.5	0.38	−2.0	−0.29	2.0×10^7	8.3×10^{-9}	1.8
16-PC*	gel	2.0	0.34	−1.5	−0.27	1.5×10^8	1.1×10^{-9}	2.0

*The parameters correspond to $T = 63$°C (as in Table IV).

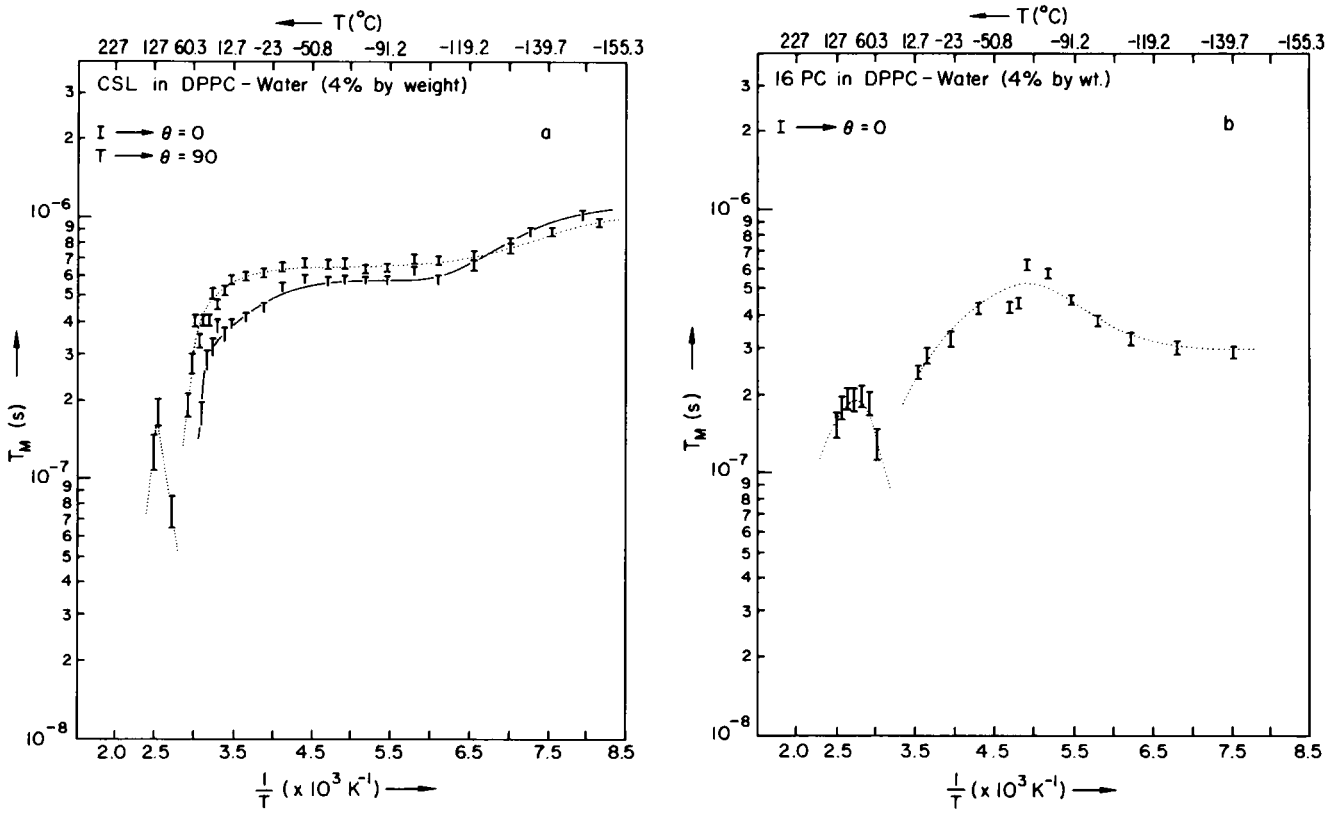

FIGURE 23 Variation of phase memory time, T_M, with sample temperature for (*a*) CSL in DPPC; (*b*) 16-PC in DPPC. The height of the symbols marking the data points (I, T) give an idea of estimated error associated with each data point. Curves (dashed for $\theta = 0°$ and solid for $\theta = 90°$) drawn through the data points are only for visual aid.

(containing only the D^2_{00} term) is not sufficient for the latter. A fair degree of asymmetry, (brought in by the $[D^2_{02} + D^2_{0\text{-}2}]$ term) must be assumed for agreement between experimental and simulated spectra. This difference in conformation of these two types of spin label, is also reflected in the orientation of their magnetic tensor axes (x''', y''', z''') with respect to the molecular ordering axes (x', y', z'): CSL exhibits y ordering (i.e. $z' \parallel y'''$), while the labeled PC probes show z ordering (i.e., z', $z' \parallel z'''$).

ESE Experiments

Fig. 23 shows the variation of the observed phase memory time T_M with sample temperature for both CSL (Fig. 23 *a*) and 16-PC probes (Fig. 23 *b*) in oriented DPPC-water multilayers. Table VI compares these experimental values of T_M with values calculated by the spectral representation method (61), using parameters estimated from cw lineshape analysis. Basically the spectral representation method entails (*a*) computation of the eigenvalues and eigenvectors of the stochastic Liouville equation of motion (SLE) using the Lanczos algorithm (1–4); (*b*) representation of the microwave radiation as a field of infinite strength and infinitesimal duration such that the sole effect of a pulse is to rotate the density matrix satisfying the SLE; (*c*) calculation of the echo amplitude or envelope corresponding to a specific pulse sequence using *a* and *b*. Since *a* is required for cw lineshape analysis described earlier, a comparison of the two sets of results (cw and ESE) is readily obtained. We first performed cw spectral simulations using a best fit procedure to estimate the parameters characterizing our system at specific temperatures (for example, the structural and motional models, λ, $R_\perp$, N, etc.). We then used the corresponding eigenvalues and

TABLE VI
COMPARISON OF EXPERIMENTAL AND CALCULATED VALUES OF PHASE MEMORY TIME, T_M FOR CSL IN DPPC + (4 wt % WATER)

Temperature	T_M (experiment)*		T_M (calculated)‡	
	$\theta = 0$	$\theta = 90$	$\theta = 0$	$\theta = 90$
C°	*ns*		*ns*	
23	528	354	49	26
46	414	176	49	21
58	399	—	39	28
68	192	—	40	36
117	178	—	51	57
129	127	—	70	76

*Estimated errors are as shown in Fig. 23 *a*.
‡Calculations use the parameters estimated from cw line shape analysis.

eigenvectors to compute T_M. From Table VII we see that the experimental and calculated values of T_M match fairly well (within a factor of 2) in the fast motional regime (where T_M decreases as the correlation time τ_R increases [61]). The fit, however, is very poor (Table VI) in the very slow motional regime (where T_M increases as τ_R increases). Use of other motional models, like the jump diffusion model, had no significant effect on T_M in this range, although the slow motional region is predicted to be model sensitive (61). To reduce the discrepancy between observed and calculated values of T_M and still retain the general features of the cw ESR spectra, we had to decrease molecular motion by about an order of magnitude and increase the ordering. Fig. 24 shows the cw spectral fits obtained in this way. The fits are seen to be qualitatively no worse than those obtained when experimental T_M values were not considered (as in Fig. 10). Apart from the molecular ordering $\langle D_{00}^2 \rangle$ and motion (R), it is found that the anisotropy parameter, $N = R_\parallel/R_\perp$ has a profound effect on T_M (calculated) (Fig. 24). These preliminary observations lead us to believe that the echo technique may give more accurate estimates of motion and motional anisotropy in the low temperature/very slow molecular motion regime. A simple 90°-τ-180°-τ-echo experiment, measuring T_M at one particular field position, is not sufficient for this purpose. Variation of T_M across the ESR spectrum can enable one to study motional effects in greater detail. Such experiments are being developed in our laboratory and preliminary results using these model membrane systems are reported elsewhere (62).

Both CSL and 16-PC show a maximum in the T_M vs. $1/T$ plot in the fast motional region. This feature has been reported earlier in egg lecithin dispersions (63). The reduction in T_M for the highest temperatures is probably due to additional relaxation mechanisms that come into effect at very fast motions, for example (*a*) Heisenberg spin exchange, and/or (*b*) spin rotational relaxation. Both mechanisms would add to the homogeneous line width, reducing T_M.

The analysis of ESE data in these complicated lyotropic

TABLE VII
COMPARISON OF EXPERIMENTAL AND CALCULATED VALUES OF T_M FOR 16-PC IN DPPC + (4 wt % WATER)

Temperature	T_M (experiment)*	T_M (calculated) ‡
°C	*ns*	
23	128	67
84	202	138
95	188	146
106	190	172
117	173	208
129	150	304

*Estimated errors are as shown in Fig. 23 *b*.
‡Calculations use the parameters estimated from cw lineshape analysis.

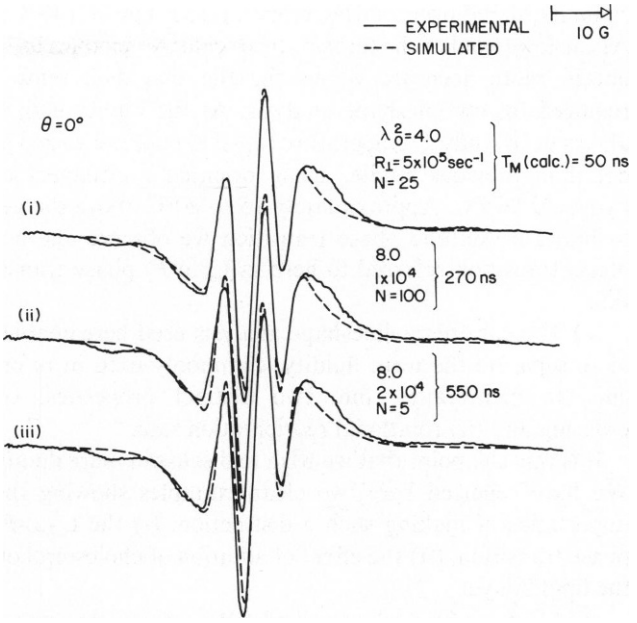

FIGURE 24 Experimental and simulated ESR spectrum for CSL in DPPC at T = 22°C. Simulation in *i* correspond to parameters arrived at by considering best fit to the cw spectrum alone; in *ii* and *iii* the simulation parameters have been chosen so that the corresponding calculated value of T_M approaches the experimentally measured value of ~500 ns at T = 22°C. $A_\perp$ used in *ii* and *iii* was 5.2 G (instead of 5.0 G, as in *i*). Note that the cw lineshapes are not significantly affected by these adjustments, i.e., from the best fit approach alone simulations in *i*, *ii*, and *iii* would be equally justified.

systems brings out three important points. (*a*) Even in the slow motional region where cw spectral simulations are still sensitive to motion, it is very difficult to obtain a unique set of parameters characterizing the system under study. (*b*) Temperature-dependent inhomogeneous broadening may dominate cw ESR lineshape in the extreme slow motional region. In cw lineshape analysis there is a danger of misintrepreting this effect to be due to motion. In ESE experiments one can measure just the homogeneous ESR linewidths, thereby obtaining greater resolution in motional information. (*c*) Close to the ESR rigid limit ($\tau_R \geq 10^{-6}$ s) ESE data may provide a useful guideline for accurate spectral analysis (62, 64).

FURTHER DISCUSSION

The detailed lineshape analysis reported here brings into focus the following points regarding ESR study of model membrane systems.

(*a*) Careful alignment of samples to obtain orientation-dependent ESR spectra greatly enhances the resolution of information, making the complicated cw lineshape analysis feasible. Since defects in alignment have a profound effect on ESR spectra (fig. 4) it is most essential to confirm the degree of macroscopic alignment using an independent technique, such as polarizing microscopy.

(*b*) Our aligned samples of low water content DPPC

remain ordered over a large temperature range (±140°C). At the lower end of the temperature scale this enables us to obtain more accurate values for the magnetic tensors required for cw lineshape analysis. At the higher end, it allows us to study a temperature range not characterized in detail in previous studies using oriented multilayers of hydrated DPPC. Approximately 15 to 20°C above the gel to liquid crystalline phase transition we observe another phase transition referred to here as L_α-to-F_2 phase transition.

(*c*) The careful cw lineshape analysis used here enables us to separate the term fluidity, commonly used in reference to membranes, into two distinct properties: (*i*) ordering and (*ii*) rotational reorientation rate.

It is this last point that we wish to discuss in more detail. We have reported here two clear examples showing the importance of making such a distinction: (*i*) the L_α-to-F_2 phase transition, (*ii*) the effect of addition of cholesterol on the lipid bilayer.

(*i*) Although qualitatively the ESR evidence (the growing in of one line synchronous with the disappearance of another) is very characteristic of a phase transition (Fig. 12), we rely more on the changes in the molecular parameters of ordering and rotational diffusion to mark a true phase transition. The Arhenius-type plots of τ_R $[\propto(R_\perp R_\parallel)^{-1/2}]$ vs. temperature consistently show two discontinuities above 22°C in every system studied; one corresponds to the well-known gel to L_α transition and the second corresponds to what we call the L_α-to-F_2 transition. The first is characterized by a relatively small reduction in ordering and a larger increase in rotational diffusion (see Table IV where the anisotropy in R does not complicate the issue). The second is characterized rather by a very large reduction in ordering and a relatively small increase in rotational diffusion. It is almost as if the first is a motional transition while the second is a structural one. Although the high temperature F_2 phase exhibits very low ordering, it is nevertheless, a smectic phase and not a nematic or isotropic one; i.e., the bilayer structure still appears to be maintained, although cooperative interbilayer forces may be small compared with the L_α and gel phases. Since this F_2 phase has not been observed before in low water content DPPC (by ESR or other techniques) we plan to confirm this in the future by an independent technique (optical and/or x-ray diffraction). Differential scanning calorimetry (DSC) performed on dispersions (or powders) do not seem to show this transition (24). It could be that the change in heat capacity involved is very small or very broad (or both) and therefore remains unresolved from the main endothermic peak corresponding to the gel-to-L_α transition. It is difficult to explain our ESR observations in any other way. We have considered and rejected a lipid-water (steam) phase separation model for the following reasons. (*i*) At the lowest water content (2% by weight) the water is associated with the DPPC molecule as a water-of-hydration. It does not seem reasonable to overcome this binding force by thermal energies alone at ~100°C. (*ii*) Even if such a phase separation does occur it is not expected to be reversible, energetically or physically (i.e., the steam would, in all likelihood, escape from the sample, making it impossible to recover the oriented lipid-water bilayer structure observed on lowering the temperature). (*iii*) Without a water interface a bilayer structure could not be maintained in the F_2 phase. However, the ESR spectra are characteristic of a smectic phase.

Biologically, this phase may be significant in that it is close to the main transition (gel-to-liquid crystalline). In complex biological membranes containing many different types of lipid molecules the main transition occurs at relatively low temperatures. Thus, the energy involved in the L_α-to-F_2 transition may be quite small. It is then interesting to speculate that for some specific functions the membrane may be pushed over from the liquid crystalline L_α phase, characterized by relatively high ordering to the F_2 phase with very low ordering, making the membrane matrix less constrained or more versatile. However, we have as yet to consider the role of the headgroup region in this transition.

(*ii*) Since sterols and phospholipids are the major components of cellular membranes, the interaction between cholesterol and DPPC has been investigated extensively (38, 65). Most studies report a critical lipid to cholesterol ratio at which a change is observed in the physical state of the membrane (or model membrane). Although cholesterol is reported to have a condensing effect in general on lipid membranes, for DPPC, in particular, cholesterol has been shown to increase membrane fluidity in the gel phase, and decrease it in the liquid crystalline phase (38, 66, 67). We find that the major effect of cholesterol on DPPC (low water content) multilayers is to increase the ordering. In the gel phase the ordering is increased to such an extent that the membrane seems to have become essentially crystallized or static (i.e., there is very small change in R as the temperature is changed). In other words the decrease in the value of R is not as overwhelming as the decrease in the rate of change of R with temperature compared with the pure lipid-water system. Increase in ordering and decrease in rotational diffusion is observed in the liquid crystalline L_α phase also. However, in the F_2 phase where a drastic decrease in ordering occurs even in the pure lipid-water system, cholesterol seems to decrease the ordering further. The rotational diffusion is increased correspondingly. So it appears as if a system, which is highly ordered to start with, undergoes a structural change (by the incorporation of a critical amount of cholesterol) making it even more ordered, and the reverse occurs if the system is weakly ordered.[2] We concur with the observation of other workers that a critical ratio of lipid to cholesterol is

[2]It is interesting to note that an opposite effect is observed on addition of small amounts of gramicidin to partially hydrated DPPC multilayers (68).

required for such a structural transition to occur. We see no effects until the ratio is increased from 40:1 to 20:1. Once this critical concentration has been reached the effect is almost concentration independent, i.e., a plateau is obtained very quickly. This has also been observed before (38). Such behavior is not unlike some enzyme-substrate interactions and it would be interesting to investigate whether a reaction site is involved. If so, it appears that it would have to be a particular molecular conformation rather than stereochemical in nature, since it has been shown previously that the rigidifying effect of cholesterol in membranes (and on DDPC in particular) does not depend on specific sites of interaction and DPPC behaves like an achiral molecule with respect to the effect of cholesterol on membranes (40).

SUMMARY

A method has been described for successful preparation of oriented lipid multilayers of thickness ≤ 400 μm. This has been shown to be very useful for ESE experiments where one currently requires $\sim 10^{16}$ spins for a good signal. Future improvements in technique (e.g., increasing signal-to-noise of the ESE spectrometer, decreasing spectrometer dead-time, etc.) could reduce this number so that it approaches the requirement for an accurate cw experiment ($\sim 10^{14}$ spins). But until then our expertise in preparing thick oriented multilayer enables us to use ESE techniques that are more sensitive for the study of molecular structure and dynamics.

Our thick (<400 μm) samples do contain a certain amount of defects ($\approx 10\%$). However, comparison with a detailed study in this lab using very thin (<10 μm) oriented lipid multilayers containing $\sim 3\%$ defects shows that results remain largely unaffected; i.e., $\sim 10\%$ defects appear to be tolerable for our present purposes.

Our low water content, oriented lipid multilayers remain stable over long periods of time and over a large range of temperature. We are, therefore, able to study the rigid limit in detail. This enables us to estimate the magnetic tensors more accurately for each lipid system and each spin label. It also gives important insights regarding the bilayer structure (e.g., hydrogen chain tilt), since the information is not complicated by motional effects.

We described our observation of a high-temperature liquid crystalline phase ~ 15 to 20°C above the previously reported gel to L_α transition. Although its biological significance is not directly apparent, the greatly reduced ordering and fast molecular motions associated with it make this an interesting smectic A phase for further study.

Our cholesterol study shows that our oriented multilayer samples are suitable systems for studying the effects of additives on hydrated lipid bilayers. By addition of polypeptides, ions, etc., these model systems may be made to reflect the complexities of a biological membrane. By orienting these liquid crystalline smectic systems we have approached the resolution obtainable from ESR studies of single crystals, yet we are able to study the molecular dynamics, which remains our primary concern. We have established that methods of analysis thus far mainly applied to thermotropic systems, are capable of handling the more complex model membrane systems. The large number of parameters involved in the simulations become meaningful only because we are able to correlate them with orientation-dependent spectra in order to approach the unique set of parameters defining the system at any particular temperature.

Lastly, we have shown that these complex lipid-water systems may be studied by ESE techniques. We plan to exploit the enhanced sensitivity to motions of the ESE technique coupled with the improved resolution due to orientation dependence of aligned samples in our future studies of model membrane systems.

This work was supported by The National Institutes of Health grant 08-RIGM-25862.

Received for publication 29 August 1984 and in final form 15 April 1985.

REFERENCES

1. Polnaszek, C. F., G. V. Bruno, and J. H. Freed. 1973. ESR lineshapes in the slow-motional region: anisotropic liquids. *J. Chem. Phys.* 58:3184–3199.
2. Freed, J. H. 1976. Theory of slow tumbling ESR spectra for nitroxides. *In* Spin Labeling, Theory and Applications. L. J. Berliner, editor. Academic Press, Inc., New York. 53–132.
3. Moro, G., and J. H. Freed. 1980. Efficient computation of resonance spectra and related correlation functions from stochastic Liouville equations. *J. Phys. Chem.* 84:2837–2840.
4. Moro, G., and J. H. Freed. 1981. Calculation of ESR spectra and related Fokker-Planck forms by the use of the Lanczos algorithm. *J. Chem. Phys.* 74:3757–3773.
5. Hwang, J. S., R. P. Mason, L. P. Hwang, and J. H. Freed. 1975. ESR studies of anisotropic rotational reorientation and slow tumbling in liquid and frozen media. III. Perdeuterated 2,2,6,6-tetramethyl-4 piperidone N-oxide, and an analysis of fluctuating torques. *J. Phys. Chem.* 79:489–511.
6. Polnaszek, C. F., and J. H. Freed. 1975. ESR Studies of anisotropic ordering, spin relaxation and slow tumbling in liquid crystalline solvents. *J. Phys. Chem.* 79:2283–2306.
7. Lin, W. J., and J. H. Freed. 1979. ESR Studies of anisotropic ordering, spin relaxation and slow tumbling in liquid crystalline solvents. 3. Smectics. *J. Phys. Chem.* 83:379–401.
8. Meirovitch, E., D. Igner, E. Igner, G. Moro, and J. H. Freed. 1982. Electron spin relaxation and ordering in smectic and supercooled nematic liquid crystals. *J. Chem. Phys.* 77:3915–3938.
9. Rao, K. V. S., C. F. Polnaszek, and J. H. Freed. 1977. ESR Studies of anisotropic ordering, spin relaxation and slow tumbling in liquid crystalline solvents. 2. *J. Phys. Chem.* 81:449–456.
10. Meirovitch, E., and J. H. Freed. 1980. ESR Studies of anisotropic ordering, spin relaxation and slow tumbling in liquid crystalline solvents. IV. Cholestane motions and surface anchoring in smectics. *J. Phys. Chem.* 84:2459–2472.
11. Meirovitch, E., and J. H. Freed. 1984. Molecular configuration, intermolecular interactions and dynamics in smectic liquid crystals from slow motional ESR lineshapes. *J. Phys. Chem.* 88:4995–5004.
12. Luckhurst, G. R. 1974. Magnetic resonance spectroscopy of liquid

crystals non-amphiphilic systems. *In* Liquid Crystals and Plastics Crystals. Vol. 2. G. W. Grady and P. A. Winsor, editors. Ellis Harwood Ltd., New York. 144–191.
13. Levine, Y. K. 1972. Physical studies of membrane structures. *Prog. Biophys. Mol. Biol.* 24:3–74.
14. Tardieu, A., V. Luzzati, and F. C. Leman. 1973. Structure and polymorphism of the hydrocarbon chains of lipids. A study of lecithin-water phases. *J. Mol. Biol.* 75:711–733.
15. Levine, Y. K. 1973. X-ray diffraction studies of membranes. *Prog. Surf. Sci.* 3:279–352.
16. Hentschel, M., and R. Hosemann. 1983. Small-and wide angle x-ray scattering of oriented lecithin multilayers. *Mol. Cryst. Liq. Cryst.* 94:291–316.
17. Sakurai, I., and S. Iwayanagi. 1981. Phase transitions in single crystals of L-DPPC and DL-DPPC. *Mol. Cryst. Liq. Cryst.* 67:89–100.
18. Büldt, G., H. U. Gally, A. Seelig, J. Seelig, and G. Zaccai. 1978. Neutron diffraction studies on selectively deuterated phospholipid bilayers. *Nature (Lond.)* 271:182–184.
19. Petrov, A. G., K. Gawrisch, G. Brezesinski, G. Close, and A. Mops. 1982. Optical detection of phase transitions in simple and mixed lipid-water phases. *Biochim. Biophys. Acta.*690:1–7.
20. Luna, E. J., and H. M. McConnell. 1977. The intermediate monolitic phase of phosphatadylcholines. *Biochim. Biophys. Acta.* 466:381–392.
21. Yellin, N., and I. W. Levin. 1977. Hydrocarbon chain disorder in lipid bilayers. Temperature-dependent Raman spectra of 1,2-diacyl phosphaticylcholine-water gels. *Biochim. Biophys. Acta.* 489:177–199.
22. Asher, S. A., R. Stearns, T. Urabe, and P. S. Pershan. 1981. Raman and x-ray studies of single crystals of dipalmitoylphosphatidylcholine. *Mol. Cryst. Liq. Cryst.* 63:193–204.
23. Chen, S. C., J. M. Sturtevant, and B. J. Gaffney. 1980. Scanning calorimetric evidence for a third phase transition in phosphatidylcholine bilayers. *Proc. Natl. Acad. Sci. USA.* 77:5060–5063.
24. Kodama, M., M. Kuwabara, and F. Seki. 1982. Successive phase transition phenomenia and phase diagram of phosphatadylcholine-water system as revealed by differential scanning calorimetry. *Biochim. Biophys. Acta.* 689:567–570.
25. Hemminga, M. A., and P. R. Cullis. 1982. ^{31}P NMR studies of oriented phospholipid multilayers. *J. Magn. Reson.* 47:307–323.
26. Trahms, L., W. D. Klabe, and E. Bokoske. 1983. ^{1}H NMR study of the three low temperature phases of DPPC-water systems. *Biophys. J.* 42:285–293.
27. Berliner, L. J., editor. 1976. Spin Labeling, Theory and Applications. Academic Press, Inc., New York.
28. Marsh, D. 1981. Electron spin resonance: spin labels. *In* Membrane Spectroscopy. E. Grell, editor. Springer-Verlag, Berlin. 51–142.
29. Hemminga, M. A. 1983. Interpretation of ESR and saturation transfer ESR spectra of spin labeled lipids and membranes. *Chem. Phys. Lipids.* 32:323–383.
30. Meirovitch, E., and J. H. Freed. 1980. An ESR spin probe study of low water content DPPC bilayers. Cooperative chain distortions. *J. Phys. Chem.* 84:3281–3295.
31. Meirovitch, E., and J. H. Freed. 1980. ESR studies of low water content, 1,2-dipalmitoyl-*sn*-glycero-3 phosphocholine in oriented multi-layers. II. Evidence for magnetic-field–induced reorientation of the polar headgroups. *J. Phys. Chem.* 84:3295–3303.
32. Taylor, M. G., and I. C. P. Smith. 1981. A comparison of spin probe ESR, ^{2}H- and ^{31}P NMR for the study of hexagonal phase lipids. *Chem. Phys. Lipids.* 28:119–136.
33. Powers, L., and N. A. Clark. 1975. Preparation of large monodomain phospholipid bilayer smectic liquid crystals. *Proc. Natl. Acad. Sci. USA.* 72:840–843.
34. Power, L., and P. S. Pershan. 1977. Monodomain samples of dipalmitoylphosphatidylcholine with varying concentrations of water and other ingredients. *Biophsy. J.* 20:137–151.
35. Powers, L. 1976. Preparation and investigation of monodomain phospholipid bilayer-water systems. Ph.D. thesis. Harvard University, Cambridge, MA.
36. Asher, S. A., and P. S. Pershan. 1979. Alignment and defect structures in oriented phosphatidylcholine multilayers. *Biophys J.* 27:393–422.
37. Stillman, A. E., L. J. Schwartz, and J. H. Freed. 1980. Direct determination of rotational correlation time by electron-spin-echoes. *J. Chem. Phys.* 73:3502–3503.
38. Smith, I. C. P., and K. W. Butler. 1976. Oriented lipid systems as model membranes. *In* Spin Labeling, Theory and Applications. L. J. Berliner, editor. Academic Press, Inc., New York. 411–451.
39. Schreier, S., C. F. Polnaszek, and I. C. P. Smith. 1978. Spin labels in practice. *Biochim. Biophys. Acta.* 515:375–436.
40. Jost, P., and O. H. Griffith. 1973. The molecular reorganization of lipid bilayers by osmium tetroxide. *Arch. Biochem. Biophys.* 159:70–80.
41. Shimoyama, Y., L. E. G. Eriksson, and A. Ehrenberg. 1978. Molecular motion and order in oriented lipid multibilayer membranes evaluated by simulations of spin label ESR spectra. *Biochim. Biophys. Acta.* 508:213–235.
42. Hemminga, M. A. 1977. Analysis of ESR spectra of the cholestane spin label in oriented multilayers of lecithin and cholesterol in the gel state. *J. Magn. Reson.* 25:25–45.
43. Koole, P., A. J. Dammers, and Y. K. Levine. 1984. Q-band electron spin resonance studies of slow motions in bilayers with high order. *Chem. Phys. Lipids.* 35:161–170.
44. Ehrstrom, M., and A. Ehrenberg. 1983. Thermal effects on motion and orientation of the cholestane spin label in planar multilayers of dimyristoylphosphatidylcholine and dipalmitoylphosphatidylcholine. *Biochim. Biophys. Acta.* 735:271–282.
45. Hubbell, W. L., and H. M. McConnell. 1971. Molecular motion in spin-labeled phospholipids and membranes. *J. Am. Chem. Soc.* 93:314–320.
46. Gaffney, B. J., and H. M. McConnell. 1974. The paramagnetic resonance spectra of spin labels in phospholipid membranes. *J. Magn. Reson.* 16:1–28.
47. Furuya, K., and T. Mitsui. 1979. Phase transitions in bilayer membranes of dioleoyl-phosphatidylcholine/dipalmitoyl-phosphatidylcholine. *J. Phys. Soc. Jap.* 46:611–616.
48. Marriott, T. B., G. B. Birell, and O. H. Griffith. 1974. Assignment of the configuration of the steroid spin label, 3-doxyl-5α-choleslane. *J. Am. Chem. Soc.* 97:627–630.
49. Dammers, A. J., Y. K. Levin, and J. A. Tjou. 1982. Computation of magnetic resonance spectra from the stochastic Liouville equation with Padé approximants. *Chem. Phys. Lett.* 88:198–201.
50. Ruocco, M. J., D. Atkinson, D. M. Small, R. P. Skarjune, E. Oldfield, and G. G. Shipley. 1981. X-ray diffraction and calorimetric study of anhydrous and hydrated *N*-palmitoylgalactosylsphingosine (cerebroside). *Biochemistry.* 20:5957–5966.
51. Ruocco, M. J., And G. G. Shipley. 1982. Characterization of the subtransition of hydrated dipalmitoylphosphatidylcholine bilayer, x-ray diffraction study. *Biochim. Biophys. Acta.* 684:59–66.
52. Johnson, M. E. 1981. Apparent hydrogen bonding by strongly immobilized spin-labels. *Biochemistry.* 20:3319–3328.
53. Janiak, M. J., D. M. Small, and G. G. Shipley. 1976. Nature of the thermal pretransition of synthetic phospholipids: dimyristoyl- and dipalmitoyllecithin. *Biochemistry.* 15:4575–4580.
54. Stamatoff, J. B., W. F. Graddick, L. Powers, and D. E. Moncton. 1979. Direct observation of the hydrocarbon chain tilt angle in phospholipid bilayers. *Biophys. J.* 25:253–262.
55. Neal, M. J., C. F. Polnaszek, and I. C. P. Smith. 1976. The influence of anesthetics and cholesterol on the degree of molecular organization and mobility of ox brain white matter lipids in multilayer membranes. A spin probe study using spectral simulation by the stochastic method. *Mol. Phamacol.* 12:144–155.
56. Worchester, D. L., and N. P. Franks. 1976. Structural analysis of

hydrated lecithin and cholesterol bilayers. II. Neutron diffraction. *J. Mol. Biol.* 100:359–378.

57. McIntosh, T. J. 1978. The effect of cholesterol on the structure of phosphatidylcholine bilayers. *Biochim. Biophys. Acta.* 513:43–58.
58. Forslind, E., and R. Kjellander. 1975. A structure model for lecithin-cholesterol-water membrane. *J. Theor. Biol.* 51:97–109.
59. Kutchai, H., L. H. Chandler, and G. B. Zavoico. 1983. The influence of cholesterol on structural order and acyl chain mobility in phosphatidylcholine multilamellar vesicles. *Biophys. J.* 41(2, Pt. 2):345*a*. (Abstr.)
60. Taylor, M. G., and I. C. P. Smith. 1980. The fidelity of response by nitroxide spin probes to changes in membrane organization. *Biochim. Biophys. Acta.* 599:140–149.
61. Schwartz, L. J., A. E. Stillman, and J. H. Freed. 1982. Analysis of electron spin echoes by spectral representation of stochastic Liouville equation. *J. Phys. Chem.* 77:5410–5424.
62. Kar, L., G. L. Millhauser, and J. H. Freed. 1984. Detection of Slow motions in oriented lipid multilayers by two dimensional electron spin echo spectroscopy. *J. Phys. Chem.* 88:3951–3956.
63. Madden, K., L. Kevan, P. D. Morse, and R. N. Schwartz. 1980. Electron spin-echo studies of nitroxide spin probes in lipid bilayers. Direct measurement of transverse relaxation times as a sensitive probe of molecular motion. *J. Phys. Chem.* 84:2691–2692.
64. Millhauser, G. L., and J. H. Freed. 1984. Two dimensional electron spin echo spectroscopy and slow motions. *J. Phys. Chem.* 81:37–48.
65. Demel, R. A., and B. de Kruyff. 1976. The function of sterols in membranes. *Biochim. Biophys. Acta.* 457:109–132.
66. Lapper, R. D., S. J. Paterson, and I. C. P. Smith. 1972. A spin label study of the influence of cholesterol on egg lecithin multilayers. *Can. J. Biochem.* 50:969–981.
67. Schreier-Mucillo, S., D. Marsh, H. Dugas, H. Schneider, and I. C. P. Smith. 1973. A spin probe study of the influence of cholesterol on motion and orientation of phospholipids in oriented multibilayers and vesicles. *Chem. Phys. Lipids.* 10:11–27.
68. Tanaka, H., and J. H. Freed. 1985. ESR Studies of lipid-gramicidin interactions utilizing oriented multibilayers. *J. Phys. Chem.* 89:350–360.
69. Guyer, W., and K. Bloch. 1983. Phosphatidylcholine and cholesterol interactions in model membranes. *Chem. Phys. Lipids.* 33:313–322.
70. Tanaka, H., and J. H. Freed. 1984. ESR Studies on ordering and rotational diffusion in oriented phosphatidylcholine multibilayers: evidence for a new chain-ordering transition. *J. Phys. Chem.* 88:6633–6644.